Eidgenössische Technische Hochschule Zürich
Swiss Federal Institute of Technology Zurich

Semester Thesis

Temperature Dependent Measurements of Undercoupled Coplanar NbTiN-Resonators

Dominik Waldburger
Spring Semester 2012

Supervisor
Tobias Thiele
Prof. Dr. Andreas Wallraff

Abstract

For the semester thesis two different sample-holder were designed. One is used to perform temperature dependent measurements of coplanar NbTiN-resonators, the other is used to couple Rydberg atoms to microwave chips. The properties of four undercoupled NbTiN-resonators were characterized as function of temperature. The critical temperature of NbTiN, the relative dielectric constant and the Q-factor of the resonators were studied analyzing the transmission spectrum of superconducting waveguides measured with a vector network analyzer.

Contents

1 Introduction

In the context of my semester project I joined the Quantum Device Lab and assisted Tobias Thiele in the "*Hybrid Cavity Quantum Electrodynamics with Atoms and Circuits*" project.

1.1 Hybrid System

The idea of a hybrid quantum system is to use the individual strengths of different quantum systems by coupling them coherently. In this experiment Rydberg atoms shall be coupled to microwave photons generated in quasi-one-dimensional coplanar microwave resonators. The long coherence time of the Rydberg atoms is thought to be used as a storage for quantum information generated e.g. in a Circuit Quantum Electrodynamics setup which is used for quantum computation. This hybrid system could be used as a quantum-RAM in a future quantum computer. Figure 1 shows the schematic of the hybrid system [1].

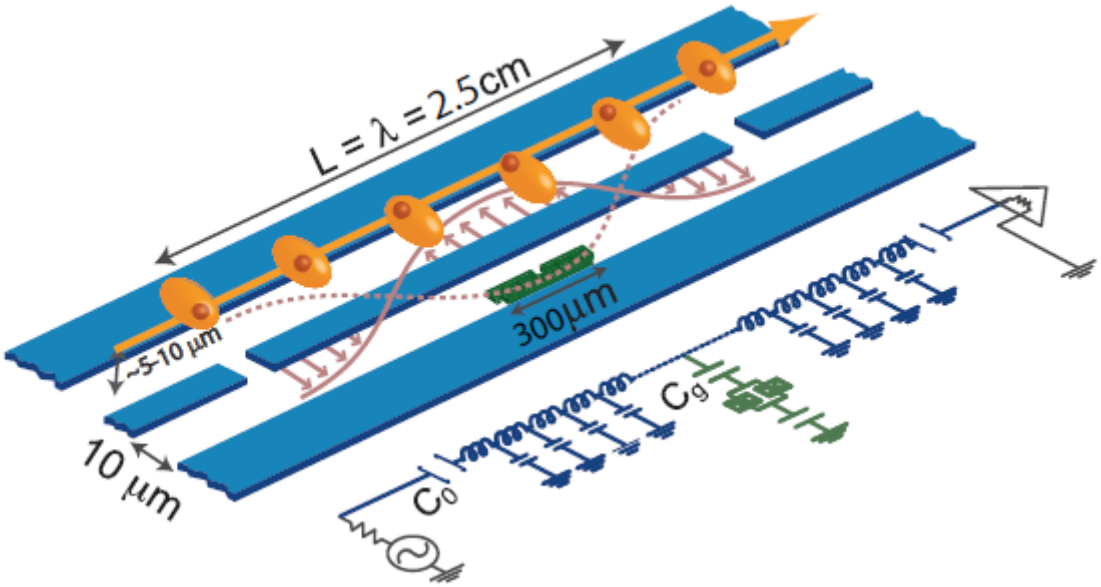

Figure 1: Schematic of a coplanar microwave resonator (blue) coupled to a superconducting qubit (green) and Rydberg atoms (orange) passing over the chip [1].

1.2 Coplanar Wave Guide

A coplanar wave guide consists of a thin (150 nm) center-conductor separated by gaps from metallic ground planes on a thick (508 μm) dielectric substrate. The waveguide has an effective dielectric constant ϵ_{eff} (1), different from the relative dielectric constant ϵ_r, depending on the geometry of the waveguide. The effective dielectric constant of a wave guide with the structure (Figure 1)

can be computed with conformal mapping techniques.

$$\epsilon_{eff} = \frac{1 + \epsilon_r \cdot K_K}{1 + K_K} \qquad K_K = \frac{K(k') \cdot K(k_2)}{K(k) \cdot K(k_2')} \tag{1}$$
$$k = \frac{W}{W + 2S} \qquad k' = \sqrt{1 - k^2}$$
$$k_2 = \frac{\tanh(\pi \cdot h \cdot S/4)}{\tanh(\pi \cdot h \cdot (S + 2W)/4)} \qquad k_2' = \sqrt{1 - k_2^2}$$

With $K(k)$ the complete elliptic integral of the first kind, h the height of the dielectric substrate, S the width of the center-conductor and W it's separation from the ground plain.
The electrical circuit of a coplanar transmission line resonator in Figure 2a) can be transformed close to a resonance mode n to an equivalent circuit shown in Figure 2b) by the following identities [2].

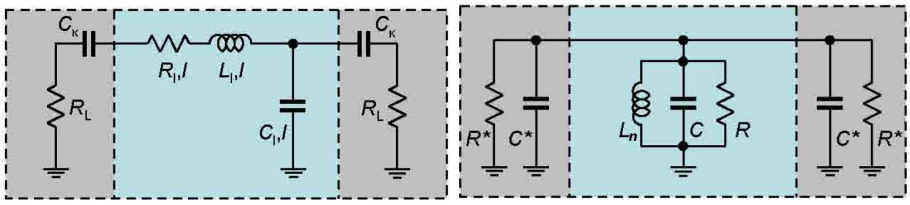

(a) (b)

Figure 2: Schematic representation of a coplanar waveguide resonator. The circuit in Figure (a) and (b) have the same properties [2].

$$L_n = \frac{2L_l l}{n^2\pi^2} \qquad \omega_n = \frac{1}{\sqrt{L_n C}} \tag{2}$$
$$R = \frac{Z}{\alpha l} \qquad R^* = \frac{1 + \omega_n^2 C_\kappa^2 R_L^2}{\omega_n^2 C_\kappa^2 R_L^2}$$
$$C = \frac{Cll}{2} \qquad C^* = \frac{C_\kappa}{1 + \omega_n^2 C_\kappa^2 R_L^2}$$

The variable α describes the attenuation constant and a finite C_κ shifts the angular frequency $\omega_n^* = \frac{1}{\sqrt{L_n(C+2C^*)}}$ of the resonator.
For a perfect isolated and lossless resonator ($C_\kappa \to \infty$, $R_l \to 0$) the transmission spectrum is discrete with the following frequencies.

$$\nu_n = n \cdot \frac{c}{2l\sqrt{\epsilon_{eff}}} = \frac{1}{2\pi\sqrt{L_n C}} \tag{3}$$

The resonances of real resonators are Lorentzian shaped and it's quality factor (4) is the quotient of the resonance frequency ν_0 and the full width half maximum $\delta\nu$.

$$L(\nu) = A_0 \cdot \frac{\delta\nu}{\delta\nu^2/4 + (\nu - \nu_0)^2} \qquad Q = \frac{\nu_0}{\delta\nu} \tag{4}$$

The Q-factor of a perfect isolated and lossless resonator can be decomposed into an external (Q_{ext}) and an internal Q-factor (Q_{int}). The quotient g (5) of Q_{int} and Q_{ext} characterizes the resonator. A resonator with $g > 1$ is called overcoupled, with $g < 1$ undercoupled and $g = 1$ defines critical coupling.

$$\frac{1}{Q} = \frac{1}{Q_{int}} + \frac{1}{Q_{ext}} \qquad g = \frac{Q_{int}}{Q_{ext}} \tag{5}$$
$$Q_{int} = \omega_n RC = \frac{n\pi}{2\alpha l} \qquad Q_{ext} = \frac{\omega_n R^* C}{2}$$

The inductance per unit length L_l (6) consist of a magnetic L_l^m and kinetic part L_l^k. The magnetic inductance L_l^m results from the geometry of the coplanar waveguide. In superconducting material appears the additional kinetic inductance L_l^k caused by the inertia of free quasi particles. The kinetic inductance L_l^k depends on the geometry of the coplanar waveguide as well as the London penetration depth $\lambda(T)$ (7). The London penetration depth is the only source of the temperature dependence of the resonance frequency $\omega_n(T)$. The dependences were given as follows [3]:

$$L_l = L_l^m + L_L^k \tag{6}$$

$$L_l^m = \frac{\mu_0}{4}\frac{K(k')}{K(k)} \qquad L_l^k = \frac{\mu_0 \cdot \lambda^2}{t \cdot W} g(S, W, t)$$

$$\lambda(T) = \sqrt{\frac{\rho(T_c)}{T_c \cdot (1 - (T/T_c)^4)}} \cdot 1.05 \cdot 10^{-3} \tag{7}$$

$$g(S, W, t) = \frac{1}{2 \cdot k^2 \cdot K^2(k)} \left(\log\left(\frac{4W}{t}\right) + k \cdot \log\left(\frac{4d}{t}\right) + \frac{2d'}{d} \log\left(\frac{S}{d'}\right) \right)$$

$$d = W + 2S \qquad d' = W + S$$

1.3 Rydberg

Rydberg atoms are exited atoms which a high principal quantum number n; such that the outer-shell electrons are far away from the nucleus. The electrons are loosely bound and their binding energy scales with n^{-2}.

$$E_n = -\frac{R_y}{(n-\delta_l)^2} \tag{8}$$

For a non hydrogen atom a correction δ_l called the quantum defect is non-zero. It is small for high angular momentum l and can be on the order of 1 or more for low l states.
Rydberg atoms have strong dipole moments (9). Due to this they are easily polarizable and there is a strong energy shift caused by external electric fields; the so called stark effect.

$$\overrightarrow{d} = e \cdot \langle \overrightarrow{r} \rangle \propto n^2 \tag{9}$$

The energy difference ΔE between neighboring states scales with n^{-3} corresponding to frequencies in the millimeter- to microwave range for $n > 25$. The lifetime t of Rydberg atoms have a n^3 dependence for low l states and a n^5 for the $l = n - 1$ state. For $n = 60$ and $l = 59$ a coherence time $\tau \approx 70$ ms can be reached [4].

E	$\propto n^{-2}$
$\overrightarrow{d}$	$\propto n^2$
ΔE	$\propto n^3$
t	$\propto n^3, n^5$

Rydberg atoms are ideal to couple to microwave resonators because of:

a) the transition frequency in the microwave range,

b) the large dipole moment favors the coupling to microwave resonators,

c) their life time is very long compared to the microwave resonators.

2 Experimental Setup

The experimental setup is based on the one described in [5]. It consists of a pulse tube cooler with two thermal shield in an ultra-high vacuum chamber. Figure 3 and 4 show the schematics and a picture of the experiment. A cold pulse of metastable helium atoms flies from the source chamber (a) through a skimmer into the experimental regime (b). There they interact with the microwaves on the chips on the sample-holder (7). Finally they are detected at an MCP (c).

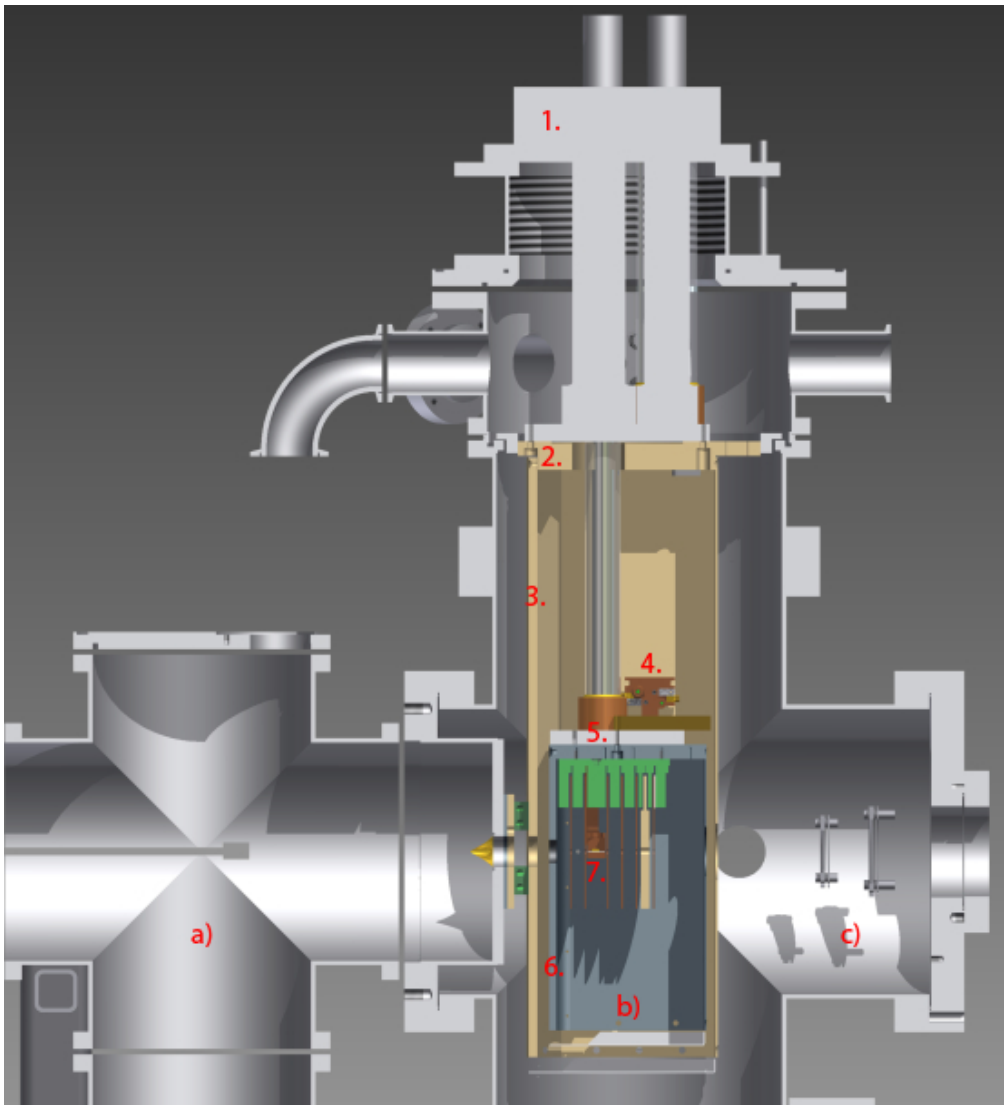

Figure 3: Schematics of the experimental setup. 1. Pulse tube cooler, 2. 40 K-stage, 3. 40 K-shield, 4. Top sample-holder, 5. 4 K-stage, 6. 4 K-shield and 7. sample-holder & electrode stack.

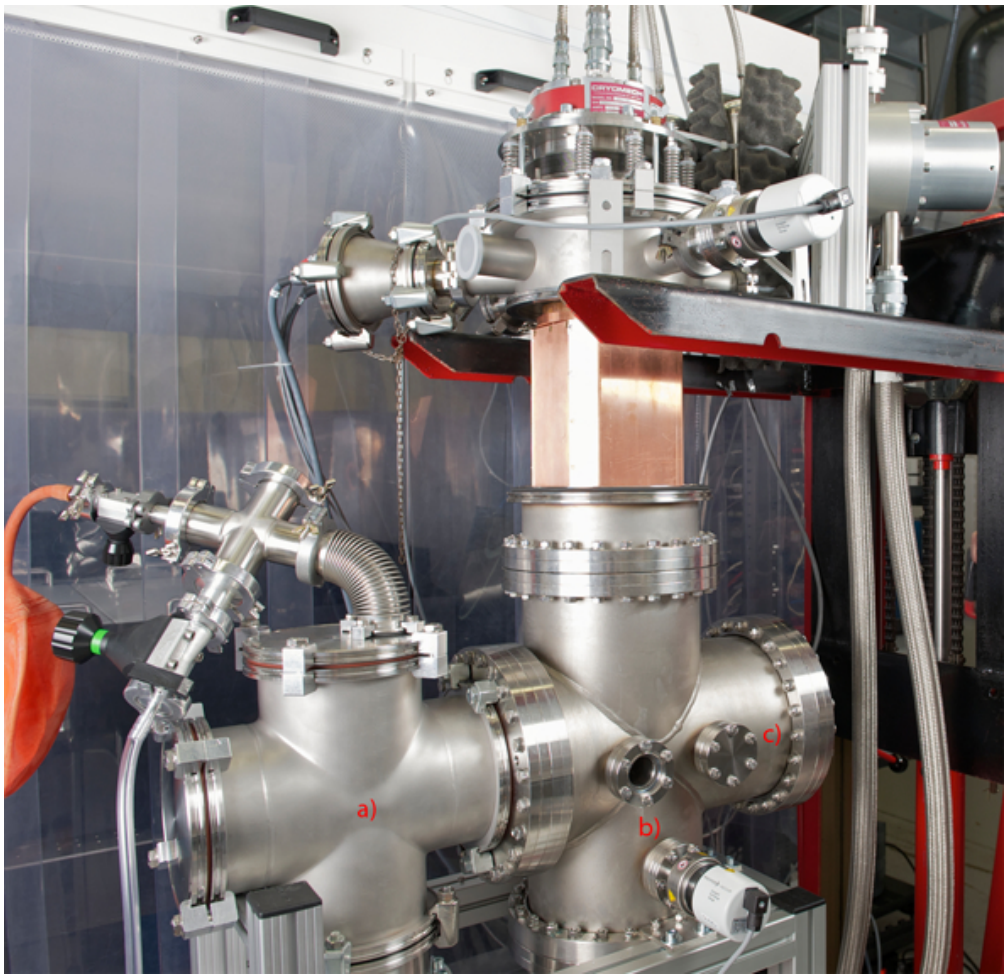

Figure 4: Picture of the experimental setup. The experiment is half open and the copper 40 K-shield is visible.

2.1 Pulse Tube Cooler & Shield

For the experiment the Cryomech PT415 Remote Motor pulse tube refrigeration system with the Cryomech CP1000 helium compressor is used. The pulse tube cooler has two cooling stages to which the two thermal copper shields are attached. A sample-cooldown is shown in Figure 5. The 4 K-stage and the top sample-holder reach a temperature of about 3 K and the 40 K-stage and 40 K-shield 32 K.
Even in the steady state there are still temperature fluctuations. The oscillations follow the frequency of the pump sound of the pulse tube cooler. With magnets and an acceleration sensor magnetic or vibrational influences were excluded. So the oscillation is an effect of the small temperature fluctuations due to the pumping of the pulse tube cooler, that have a strong effect because of good thermal coupling. The temperature oscillations are in the amplitude of 100 mK and illustrated in Figure 6.

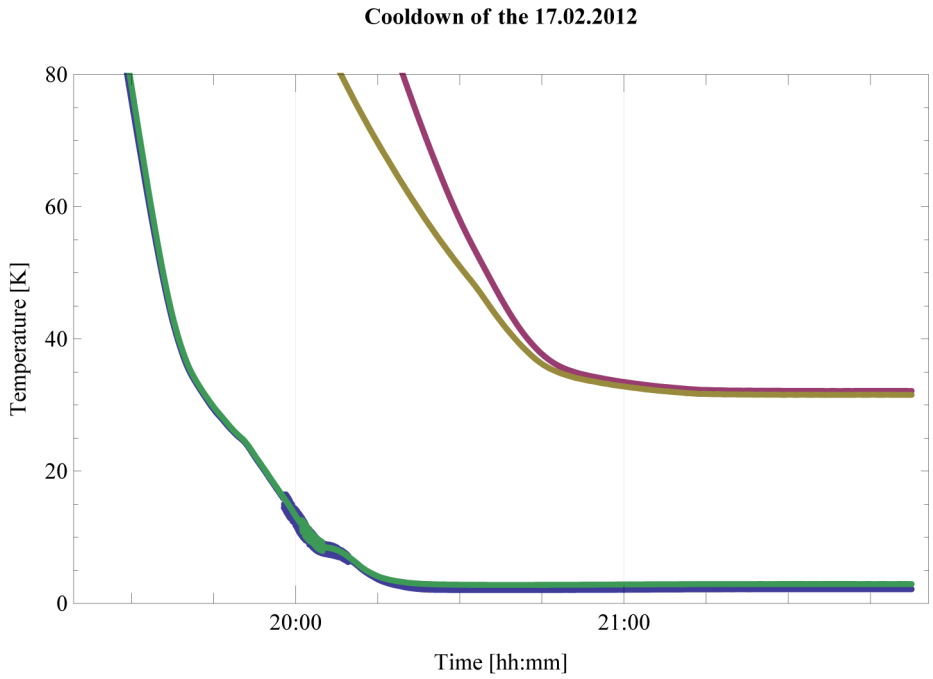

Figure 5: Cooldown of the 17.02.2012. 4 K-stage (blue), top sample-holder (green), 40 K-stage (olive) and 40 K-shield (magenta).

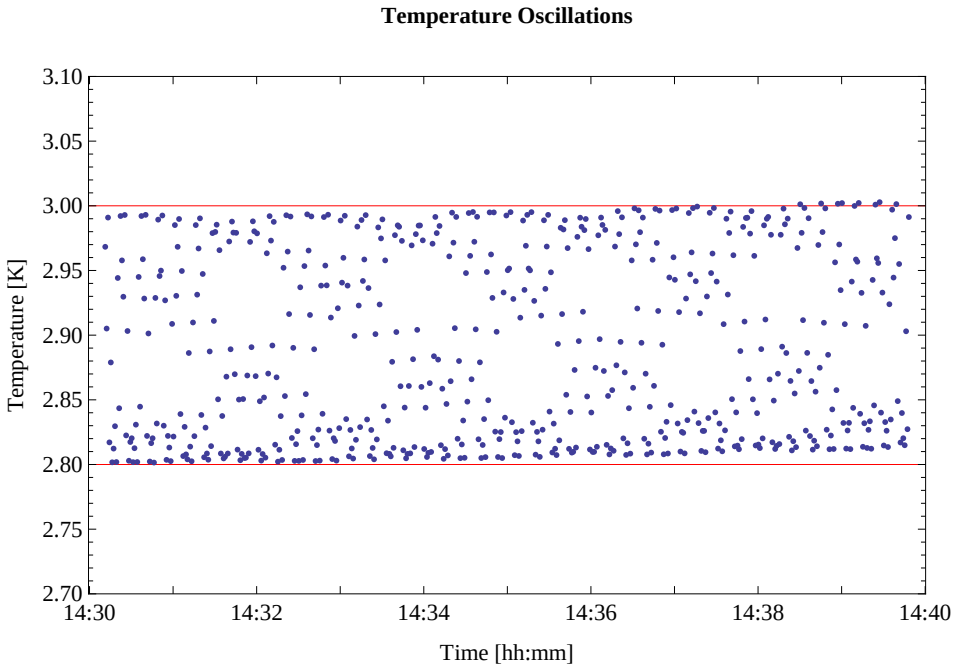

Figure 6: Temperature oscillations of the pulse tube cooler in the steady state.

2.2 Temperature Controller & Sensor System

For the temperature measurement, silicon diode sensors LakeShore DT-670C-Cu are used [6]. The sensors are placed on the 40 K-stage and -shield, on the 4 K-stage and on the top sample-holder, designed in this thesis.
The temperature controller LakeShore Model 340 [6] controls the temperature with a proportional-integral-derivative PID controller (10).

$$P_{Heater} = P\left(e + I\int e \cdot \mathrm{d}t + D\frac{\mathrm{d}e}{\mathrm{d}t}\right) \tag{10}$$

The variable $e = T_s - T_c$ describes the current error where T_s is the set-point and T_c the current temperature, P is the proportional, I the integral and D the derivative term.
The temperature controller has two feedback heater loops and can readout up to eight temperature sensors. Heater loop 1 has a maximum power output of 10 Watt and loop 2 has a maximum of 1 Watt with a 100 Ω heat resistance.
Because of the good coupling the temperature of the sample-holder respond very fast and the new temperature stabilizes within a minute. Figure 7 shows the temperature characteristics during temperature regulation.
The D-parameter is set to zero because otherwise the temperature overshoots too much. The following setting for the PID-parameters were used:

P	I	D
800	500	0

2.3 Microwave Setup

To study the properties of the transmission spectrum of the superconducting waveguide a vector network analyzer (VNA) ZVK Vector Network Analyzers produced by Rhode und Schwartz is used. The VNA sweeps the frequency over a range from 10 MHz to 40 GHz and measures S-parameters with a maximum of 1600 points per sweep and a minimal resolution of 10 Hz. The measurements can be averaged point- or sweep-wise. The number of measurements, over with the average is taken, can be set by the average factor. An output power of -10 dB is used.
The microwave signal is guided with two 50 Ω coax-cables between the VNA and the vacuum-chamber. In the vacuum-chamber there are semi-rigid coax cables connected to the PCB on the top sample-holder. From room temperature stainless steel semi-rigid coax cables are connected to 10 dB attenuators, which are then connected to the sample-holder with copper cables. The attenuators are connected to the cold head (4 K) and thermalize the center conductor of the coax cable.

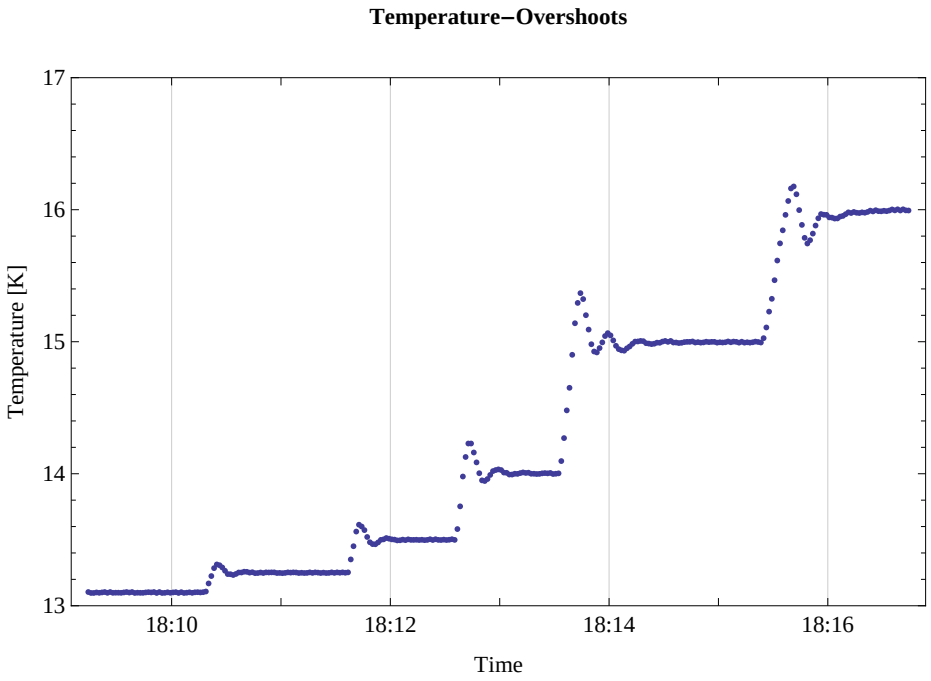

Figure 7: Temperature regulation of the top sample-holder. The target temperature is achieved after few oscillations.

2.4 Sample-holder

The goal of the new sample-holder is to achieve good thermal coupling to the 4 K stage in order to achieve minimum temperature. As material oxygen-free high thermal conductivity (OFHC) copper is chosen because of high thermal conductivity also at low temperatures. Figure 16 shows the temperature dependence of the thermal conductivity compared to other materials. To avoid reduction of the cooling power created in joints, the sample-holder arm (a) is made of one single piece. The PCB (b) holding the NbTiN chip is clamped onto the copper using a bridge (c). The plates (d) restrict the atoms to 1 mm above the chip The sample-holder is compatible with the straight and diagonal PCB designs.
The sample-holder is produced in the physics workshop of ETH Zurich and gold coated by Collini AG in Dübendorf for better reflectivity.
Building in the sample-holder it was detected that it touches an electrode. So one edge had to be milled out.
The following Figures 8 - 11 show the schematic and pictures of the sample-holder.

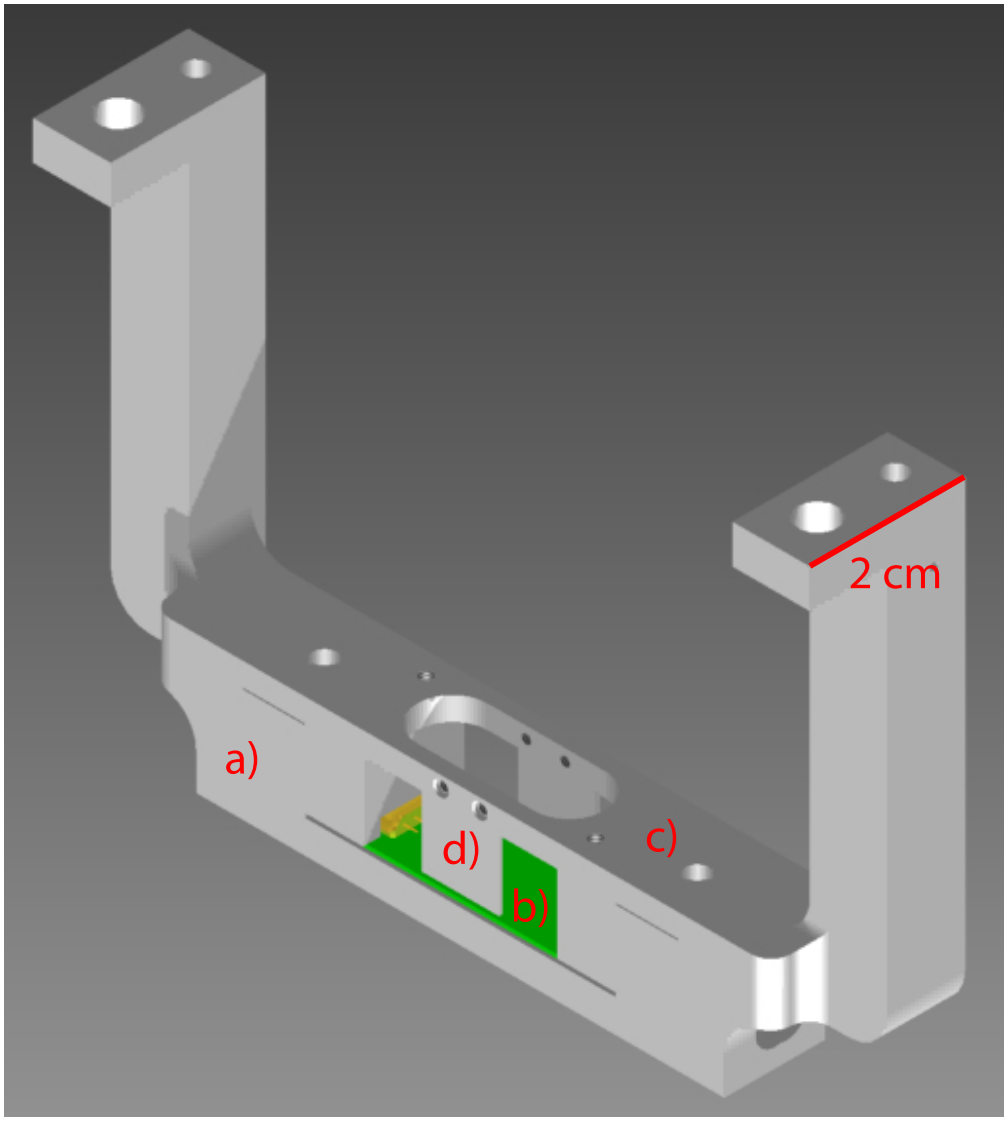

Figure 8: CAD drawing of the sample-holder. (a) the sample-holder arm, (b) the PCB, (c) the sample-holder arm and (d) shielding plates.

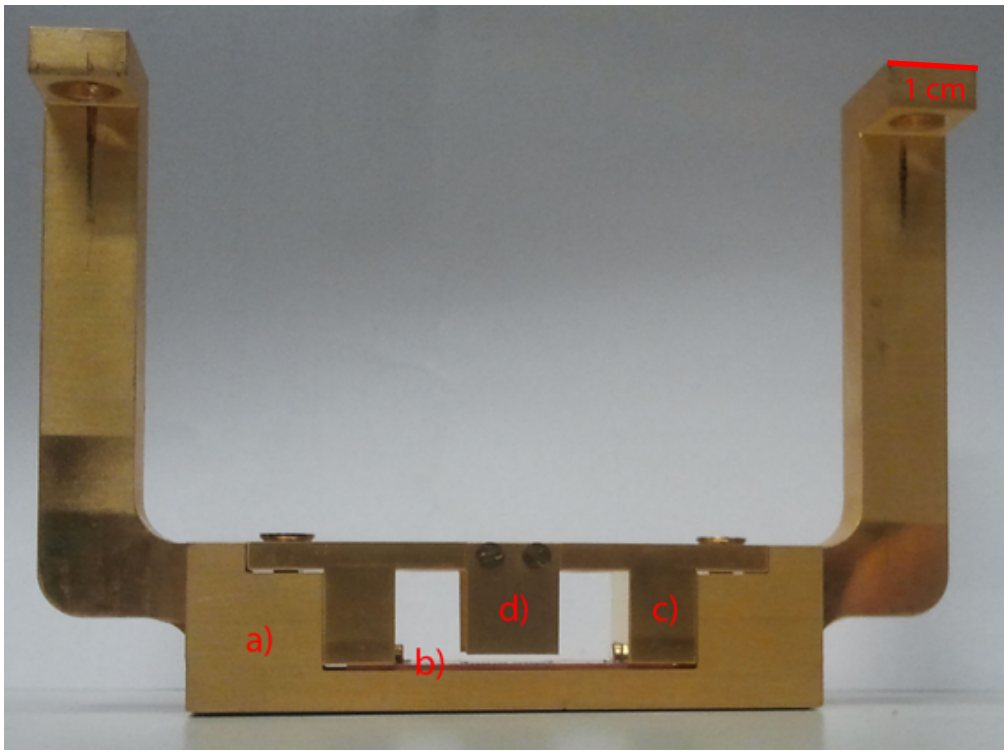

Figure 9: Picture of the sample-holder, side-view.(a) the sample-holder arm, (b) the PCB, (c) the sample-holder arm and (d) shielding plates.

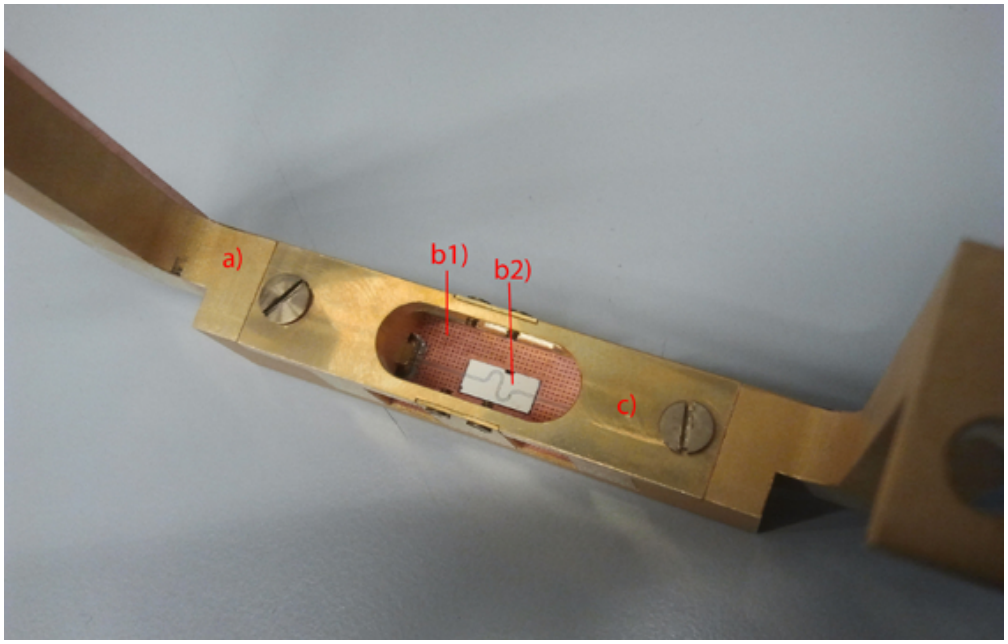

Figure 10: Picture of the sample-holder, top-view. (b1) shows the PCB with the NbTiN chip (b2).

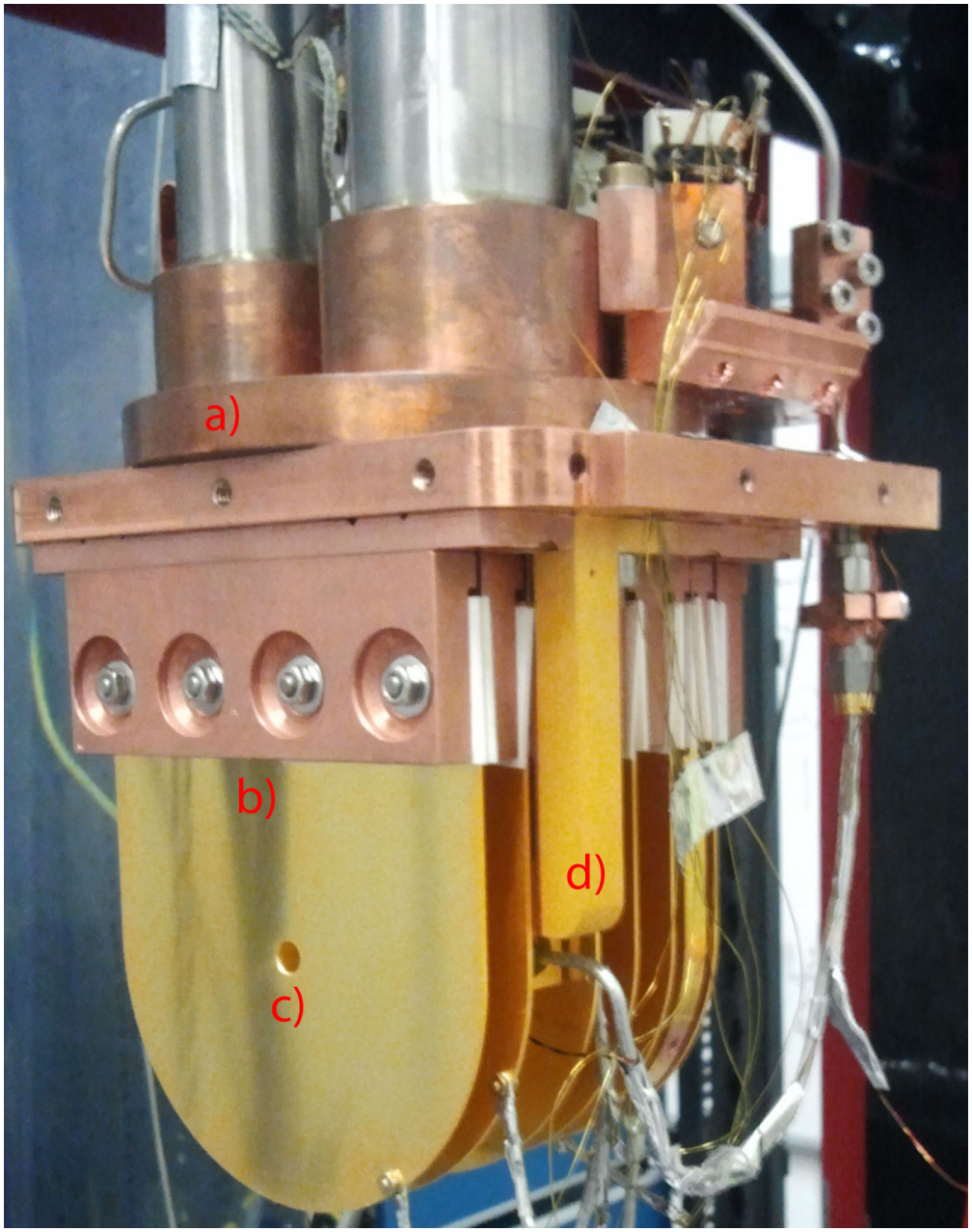

Figure 11: Picture of the sample-holder build in to the experiment. (a) cold head, (b) electrode stack with 7 electrodes, (c) hole for the atoms and (d) sample-holder.

2.5 Top Sample-holder

For temperature dependent measurements an additional sample-holder with a heater is required. The aim is to vary the temperature from 4 to 15 K, because the critical temperature of the superconducting material on the chips (NbTiN) is about 13.1 K. This should be done by dissipating 1 Watt in the heater. For this the chip must be thermally isolated so that the heating power of 1 Watt is enough, but it should not be too isolated to achieve an acceptable cooling time. Figure 12 and 13 show the design of the sample-holder. The heater consists of silk-isolated manganin resistance-wire with a resistance of 100 Ω adjusted to achieve the maximum heating power of 1 Watt.

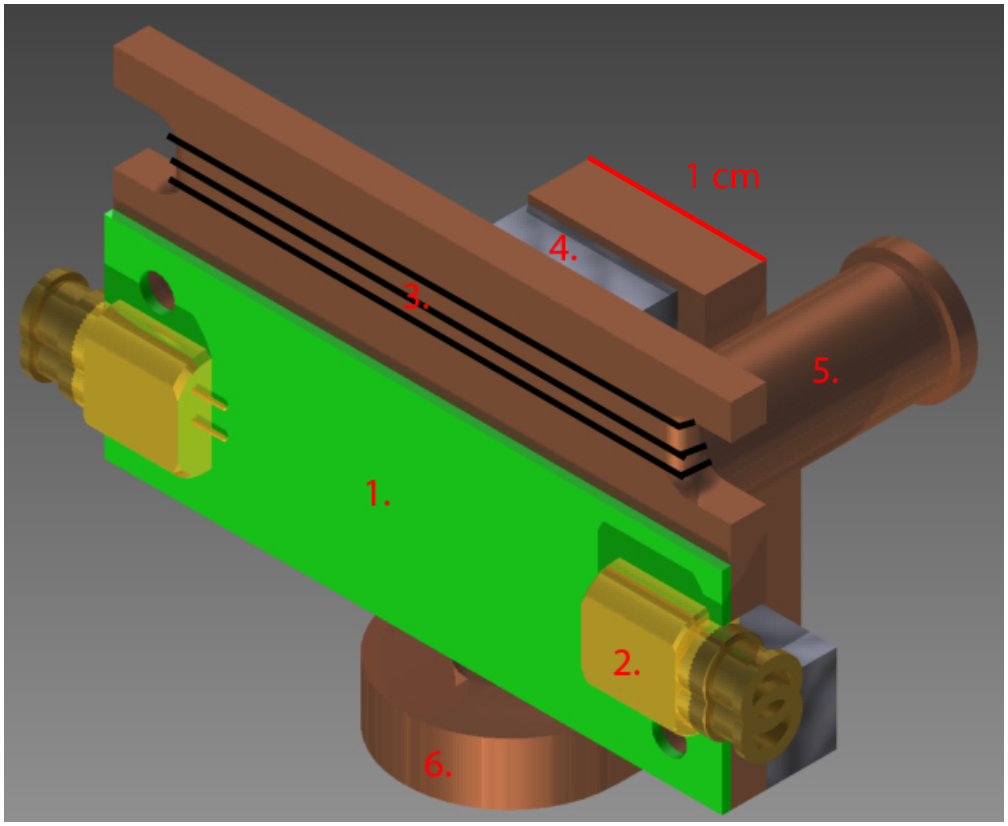

Figure 12: Front-side of the top sample-holder. 1. PCB with Chip, 2. Coaxial Print Connectors for the straight and diagonal chip design, 3. heating-wire, 4. thermal isolator, 5. thermalization of sensor and 6. socket.

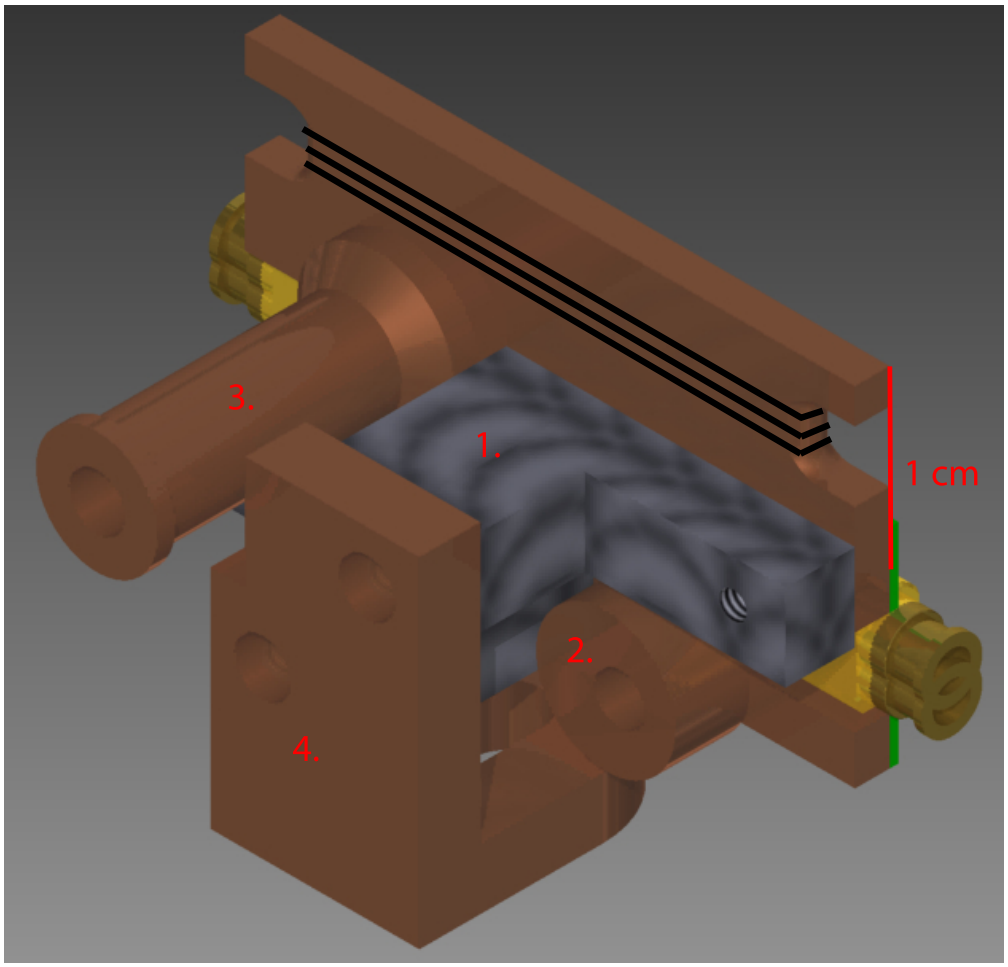

Figure 13: Back-side of the top sample-holder. 1. thermal isolator, 2. temperature sensor, 3. thermalization of sensor and 4. socket.

To estimate the dimension of isolation the following assumptions illustrated in Figure 14 and 15 are taken:

a) The only temperature gradient is over the isolating material.

b) The temperature drop over the isolating material ranges from 4 K on the cooling plate side to the wanted temperature on the chip and heater side.

c) The heat flow through the cables is neglected.

d) For the radiation from the 40 K-shield to the sample-holder blackbody radiation (11) is assumed and from the design we can neglect effects on the sides if the sample-holder and only the front- and backside are taken into account.

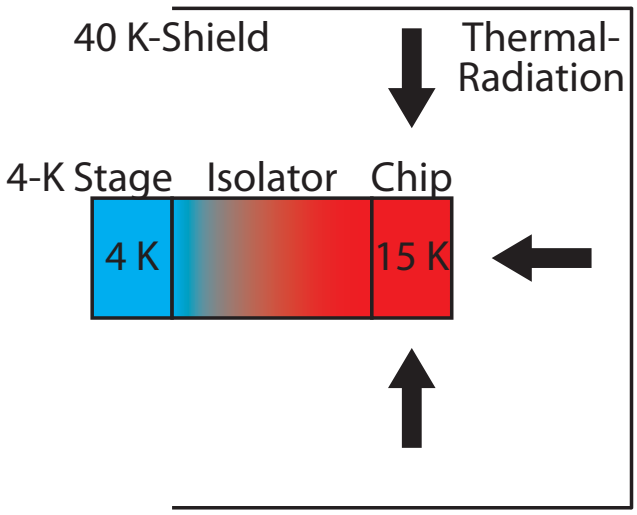

Figure 14: Schematic of the model for the calculation.

$$P_{\mathrm{d}\Omega\mathrm{d}A} = \frac{8\pi^5 k_B^4}{15c^2h^3} T^4 \frac{\mathrm{d}\Omega}{4\pi} \mathrm{d}A \cos\vartheta \tag{11}$$

Where T is the temperature, $\mathrm{d}\Omega$ the solid angle and $\mathrm{d}A\cos\vartheta$ the surface element under the angle ϑ.
As simplification the 40 K-shield and the sample-holder were considered as parallel planes. The thermal radiation form the 40 K-shield to the sample-holder is calculated by (12) and is $0.15 \cdot 10^{-3}$ Watt. The variables are illustrated in Figure 15 and have the following values.

$$P = \frac{8\pi^5 k_B^4}{15c^2h^3} T^4 \int_{-w}^{w} \int_{-h1}^{h2} \frac{A}{4\pi} \left(\frac{d1^2}{(x^2+y^2+d1^2)^2} + \frac{d2^2}{(x^2+y^2+d2^2)^2} \right) \mathrm{d}x\mathrm{d}y \tag{12}$$

T	w	$h1$	$h2$	A	$d1$	$d2$
40 K	6.3 cm	4.1 cm	∞ cm	8 cm^2	1.1 cm	12.3 cm

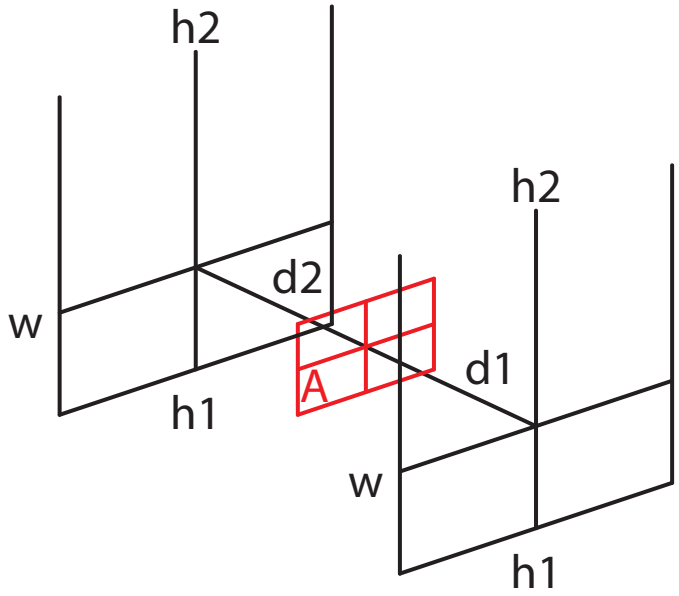

Figure 15: The sample-holder-plane with area A (red) is enclosed between the two 40 K-shield-planes (black).

The Fourier's law (13) is used to calculated the heat flow through the isolating material. The isolating material has a non-trivial shape as pictured in Figure 13, so the Fourier's law cannot be applied directly. By approximation the mean of the heat flow through the area on the 4 K-shield's side and the chip's side is used. The temperature dependence of the thermal conductivity $k(T)$ is taken from [7] and illustrated in Figure 16. In the beginning we decided for 304 stainless steel as isolation material.

$$\frac{\partial Q}{\partial t} = -k(T) \oiint_S \vec{\nabla} T \cdot \overrightarrow{\mathrm{d}A} \tag{13}$$

In the experiment the 4 K-stage reaches a temperature of 2.8 K, but the chip only 6.7 K. This equates to a external heat flux of $27.9 \cdot 10^{-3}$ Watt instead of $0.15 \cdot 10^{-3}$ Watt estimated from the thermal radiation of the 40 K-shield. This mismatch could be caused by:

a) The thermal conductivity can vary about 50% at low temperature due to slight material differences [7].

b) Through junctions the cooling power is reduced.

c) The radiation of the 40 K-shield-side-plates and the heat flux through the cables are neglected.

To reach a lower temperature of the chip the isolating part is replaced with a replica made of OFHC copper. So a minimum temperature of 2.8 K and with 1 Watt heating power a maximum temperature of 9.4 K is reached. To exceed the critical temperature of the superconducting material the heater is powered with the limit of 10 Watt.

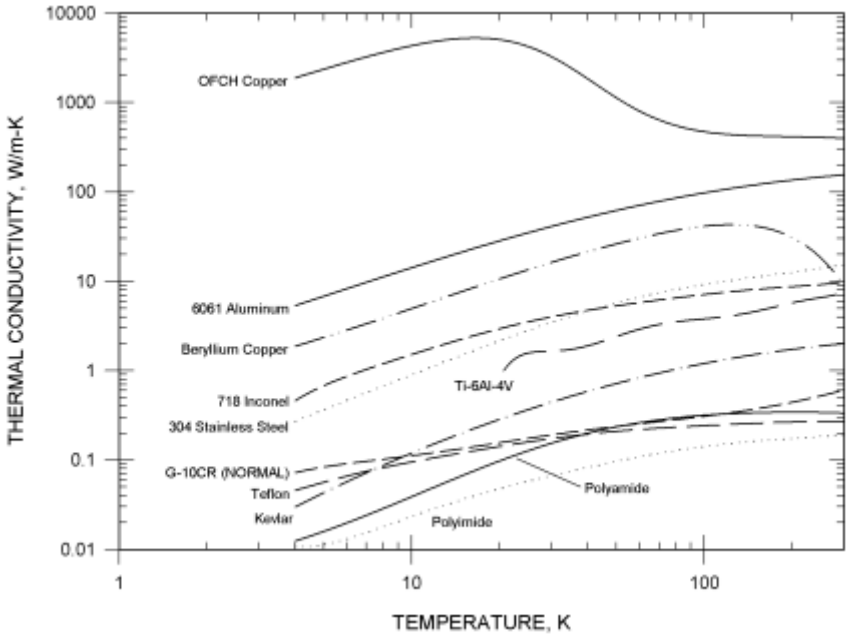

Figure 16: Thermal conductivity of various materials [7].

2.6 Chips

Four different chips named G5A2, G6O2, W1C1 and V1C2 were studied. The W1C1 and the V1C2 are a newer generation of chips than the G5A2 and the G6O2 which were characterized by Raphael Barmettler [8].
In our experiment the conducting material is Niobium Titanium Nitride (NbTiN) with a critical temperature $T_c \approx 13.1$ K. Sapphire is used as dielectric substrate with a dielectric constant $\epsilon_r \approx 10$.
In Figure 18 - 20 show the PCB and chip of W1C1. The dimension and properties of the four chips are given as followed.

Chip	Capacity [fF]	Length [mm]
G5A2	3.3	7.196
G6O2	0 (through)	8.969
W1C1	0.5	12.365
V1C2	1	12.488

S	W	t	h
160 μm	80 μm	0.15 μm	508μm

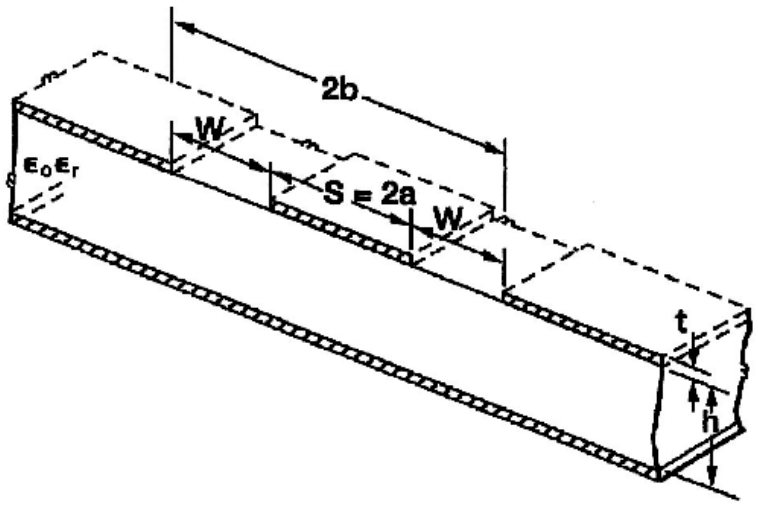

Figure 17: Characteristic of the coplanar waveguide [9].

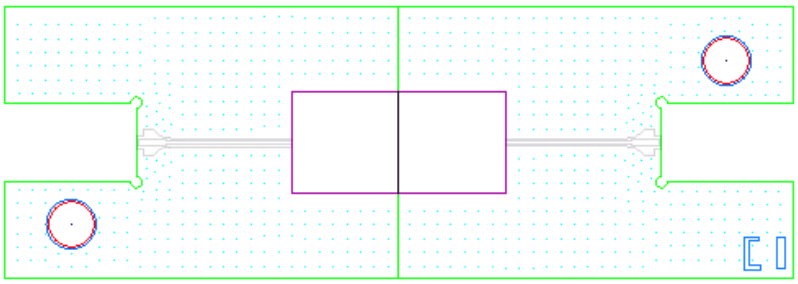

Figure 18: Schema of the PCB C1. The superconducting chip of Figure 19 is glued to the violet rectangle.

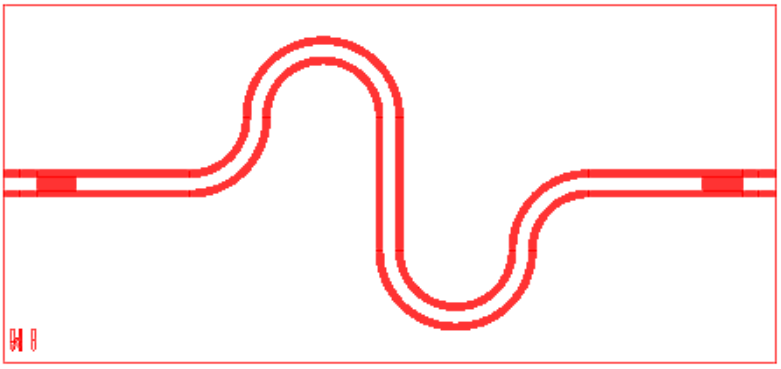

Figure 19: Schema of the superconducting NbTIN chip W1.

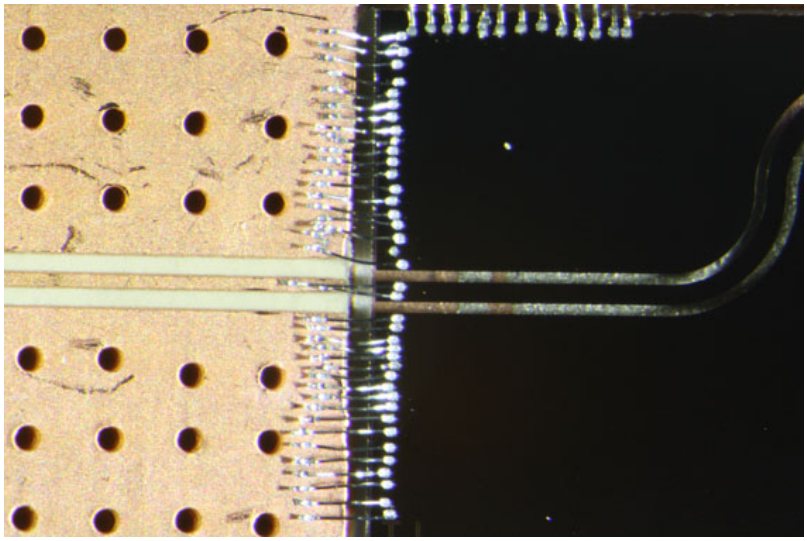

Figure 20: Picture of the bondings connecting the center conductor and the ground of the chip and the PCB.

3 Measurements & Results

3.1 Power Dependence of a Resonance

The first resonance peak of the G5A2 is measured for various power of the microwave signal. As illustrated in Figure 21 there is no change in the shape of the resonance and therefore no saturation effects. For the further measurement a power of −10 dBm is used.

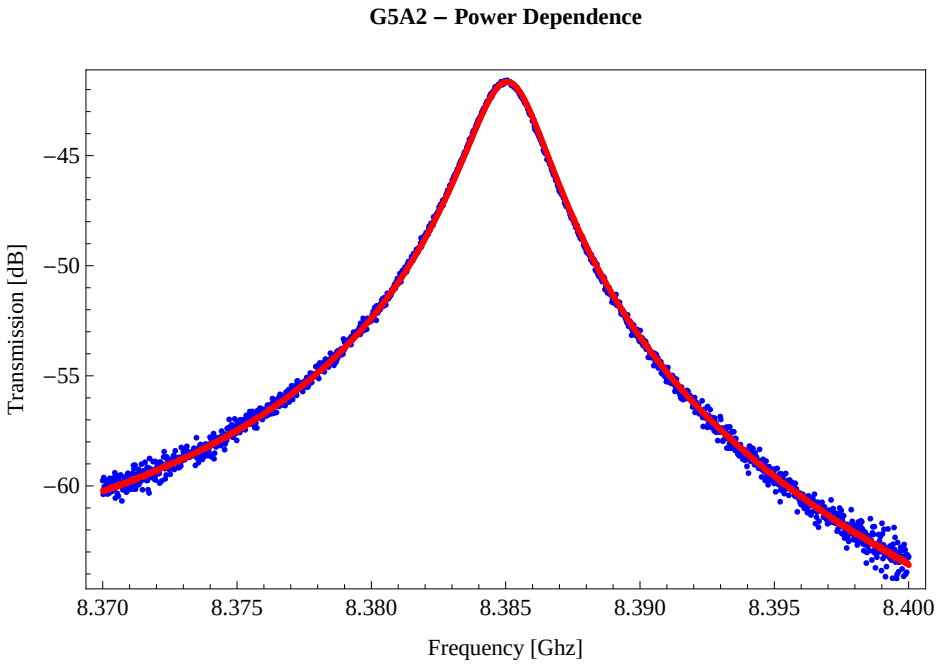

Figure 21: The first resonance of G5A2 measured with −10 dBm (red) overlaps exactly the one with −30 dBm (blue).

3.2 Temperature Dependence of the Transmission

The chip G6O2 is used to explore the temperature dependence of the transmission over the hole spectrum (10 MHz to 40 GHz) and from 3.5 to 15 K visualized in Figure 22. The visible resonances are unwanted and results from the PCB. The transmissions are fitted with the following function containing the temperature dependent fit-parameters $a(T)$ and $b(T)$. The function is chosen according to the loss in coax cables described in [10]. The -20 dB derives from the two 10 dB attenuators.

$$s21(\nu, T) = -a(T) \cdot \nu^{b(T)} - 20 \text{ dB} \tag{14}$$

Figure 23 and 24 show the temperature dependence of the fit-parameters $a(T)$ and $b(T)$ fitted with a Heaviside-function. A clear step at $T_c = 13.(1)\ K$ is visible.

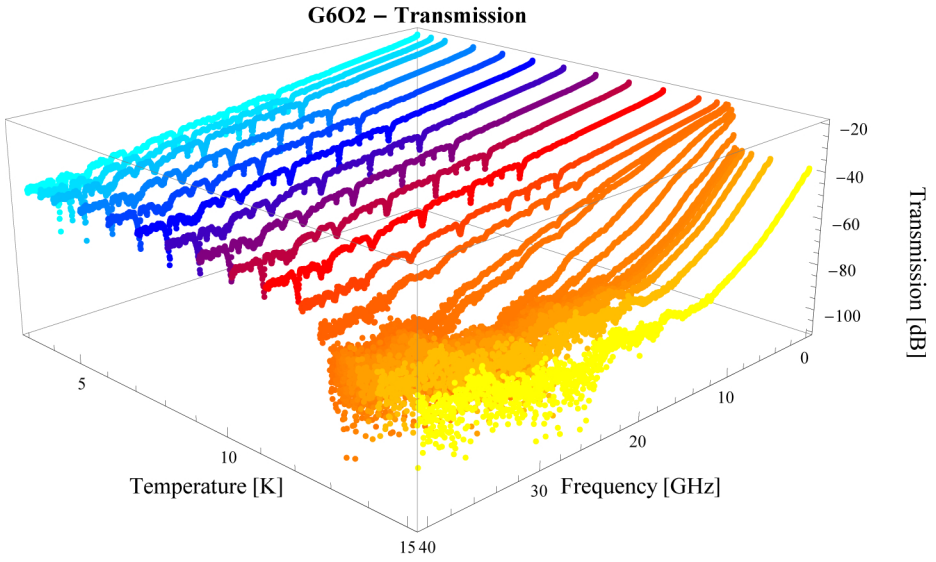

Figure 22: Dependence of the transmission as a function of the temperature and the frequency (G6O2).

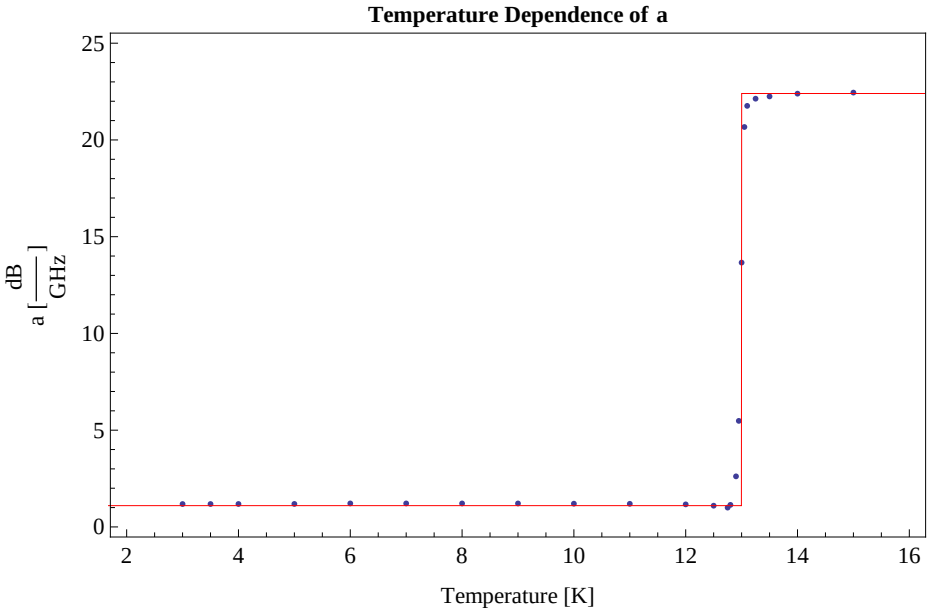

Figure 23: Temperature dependence of the fit-parameter $a(T)$.

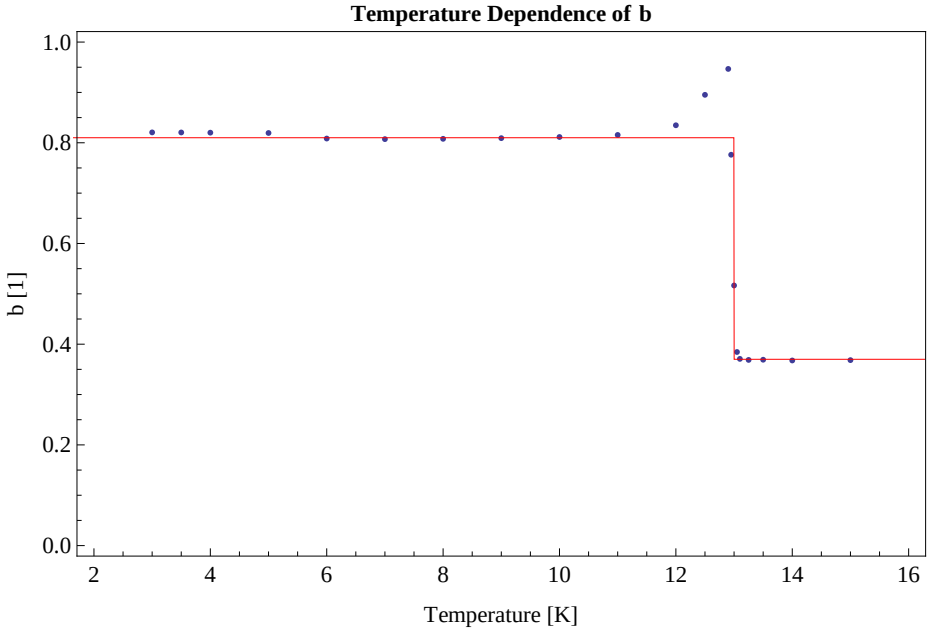

Figure 24: Temperature dependence of the fit-parameter $b(T)$.

3.3 Critical Temperature of the Superconducting Material

With a DC-resistance and a time-correlated temperature measurement the critical temperature of the superconducting material is determined. For each resistance data-point the corresponding temperature at the time of the resistance measurement is taken. For this purpose the temperature measurement is fitted with spline interpolation. The used Mathematica code is printed in the appendix B.
Figure 25 shows the step of resistance at the critical temperature. The resistance is fitted with the Fermi-Dirac-distribution (15). With $A = 114.4\ \Omega$, $B = 34.1\ \Omega$, $C = 0.01$ and the critical temperature T_c is within the range from 12.95 to 13.05 K. The width of the transition can be accounted to temperature fluctuation as well as an offset from external magnetic fields.

$$R(T) = A - \frac{B}{e^{(T-T_c)/C} + 1} \tag{15}$$

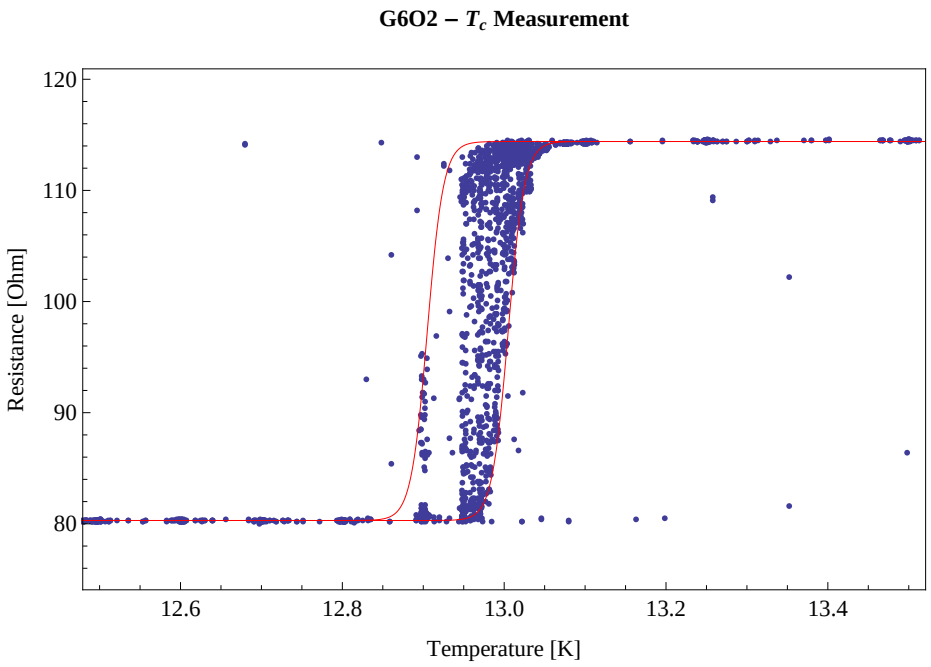

Figure 25: Temperature dependence of the resistance.

3.4 Temperature Dependence of the Resonances

3.4.1 Measurement

For the chips G5A2, W1C1 and V1C2 the resonances were measured for different temperatures from 2.8 to 12 K. The measurement is averaged either sweep- or point-wise with an average-factor of 20.

3.4.2 Fit of the Resonances

The measurement recorded in dB is first transformed back and fitted with a Lorentz-function (Equation 16). For an approximation of the quality of the fitting a second fit performed in dB (Equation 17) is done leading to a different weighting. The Mathematica code for the fits is in the appendix B. Figure 26 shows an example of a fit. The center frequency $\nu 0$ and the Q-factor of the resonance is extracted from the fit. The plots of $\nu 0$ and the Q-factor of the different chips are in the appendix A.

$$L(\nu) = \frac{A}{2\pi \cdot Q \cdot \nu 0} \frac{1}{(\frac{\nu}{\nu 0} - 1)^2 + \frac{1}{4}(\frac{1}{Q})^2} \tag{16}$$

$$L_{dB}(\nu) = 10 \cdot \log_{10}(L(\nu)) \tag{17}$$

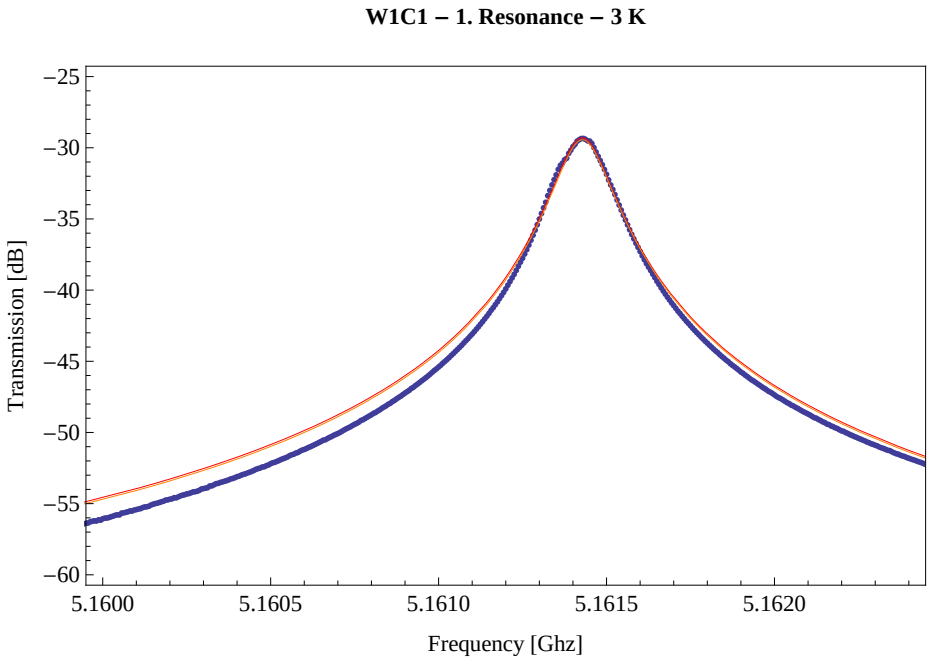

Figure 26: Fit of the Lorentz-function (red) and the Lorentz-dB-function (orange). Sweep-wise average.

3.4.3 Oscillations & Separation

By the measurement of the W1C1 chip oscillation of its frequency were observed. Therefore further measurements of V1C2 were averaged point-wise. To separated a left and right limiting curve, first the upper and lower parts of the oscillation are taken. And then split at the maximum, top-left and bottom-right points are jointed to the left and the bottom-left and the top-right to the right curve. The data points of the right curve are used for the fit with the Lorentz-function. Figure 27 shows the result of the separation and the fit. The Mathematica code of the separation is in the appendix B.

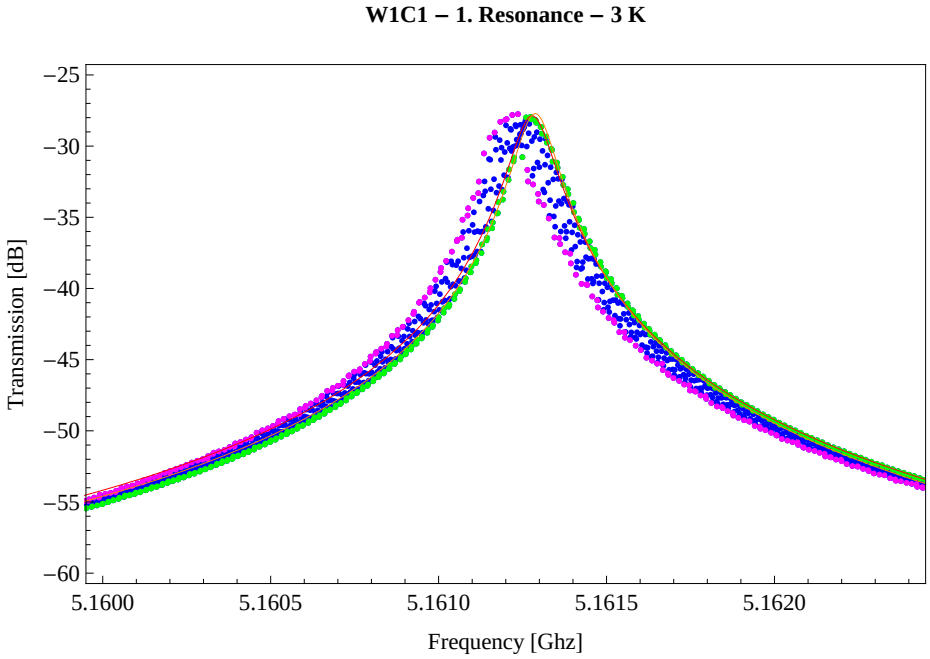

Figure 27: Separation and the fit of the oscillations. Measurement points (blue), left curve (violet), right curve (green), Lorentz-Fit (red), Lorentz-Fit-dBm (orange). Point-wise average.

3.4.4 G5A2 (critical coupled resonator, $\nu_0 = 8.385$ GHZ)

The G5A2 is measured with sweep-wise average. The first resonance of G5A2 interferes with a temperature-invariant, stationary resonance shown in Figure 28. Resulting in a faulty Q-factor for 6.5 to 10 K. The temperature dependence of the $\nu 0$ and the Q-factor for the 1^{st} to 4^{th} resonance are in the appendix A.

3.4.5 W1C1 (undercoupled resonator, $\nu_0 = 5.161$ GHz)

A double resonance is observed for the third resonance of W1C1 and illustrated in Figure 29. The temperature dependence of the $\nu 0$ and the Q-factor for the 1^{st} to 4^{th} resonance are in the appendix A.

3.4.6 V1C2 (undercoupled resonator, $\nu_0 = 5.053$ GHz)

The temperature dependence of the $\nu 0$ and the Q-factor for the 1^{st}, 2^{nd}, 4^{th} and 6^{th} resonance are in the appendix A. The 3^{rd} and 5^{th} resonances are not visible and assumed to be double-resonances as the 3^{rd} of W1C1. This could be a consequence of the asymmetric chip design (Figure 19) as a similar effect is observed for even resonances with symmetric chip designs.

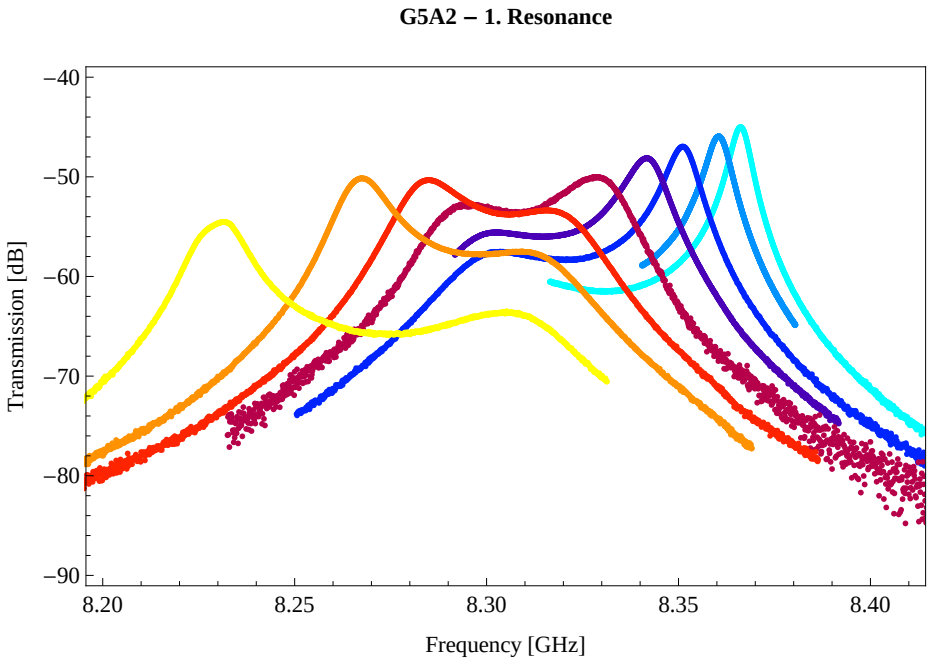

Figure 28: Interference of the first resonance with a temperature-invariant resonance. The colors indicate the different temperatures from 6.5 (blue) to 10 K (yellow).

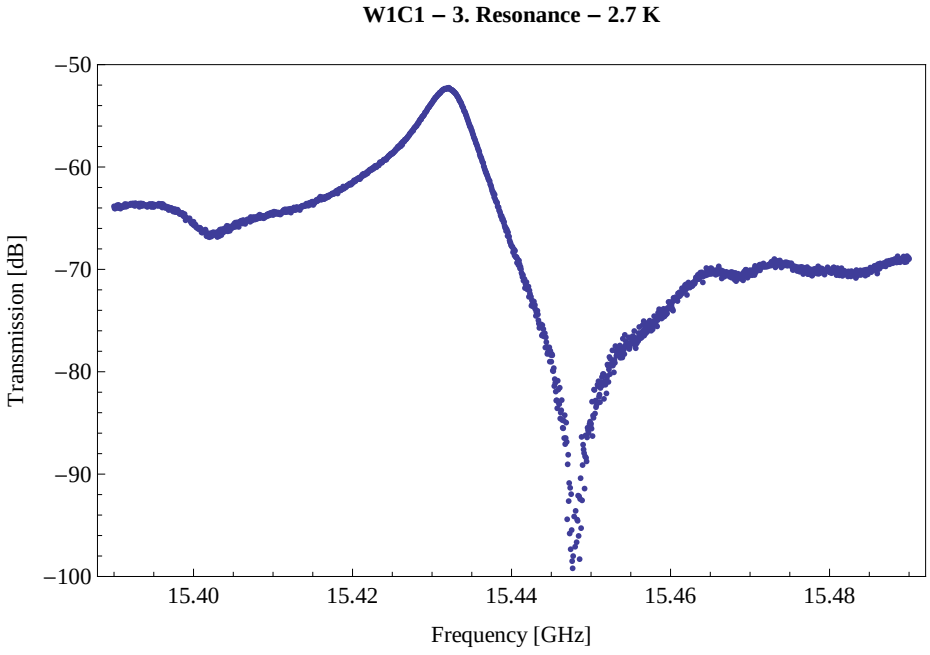

Figure 29: The double resonance of the third resonance.

3.5 Temperature Dependence of Quality Factor

According to [11] the Q-factor saturates at low temperatures. Therefore the Q-factor of W1C1 and V1C2 are fitted by (18) with the fit-parameters A, B and the saturated Q-factor Q_{sat} at T=0. The plots of the fits are in the appendix A.

$$Q(T) = \frac{Q_{sat}}{\exp\left(-\frac{T^{-1}-A}{B}\right)+1} \tag{18}$$

The saturated Q-Factor Q_{sat} is fitted with the following fit-functions (19) dependent of the resonance mode n, Figure 30 and 31. The $3rd$ resonance of W1C1 is the mentioned double-resonance and is skipped form the fitting.

$$Q_{sat}(n) = a \cdot e^{-b \cdot n} \qquad Q_{sat}(n) = c \cdot n^{-d} \qquad Q_{sat}(n) = e \cdot (n-f)^2 \tag{19}$$

The coupling ratio g (20) is computed with $Q(n)$ and Q_{ext} for G5A2 (Figure 32 and 33) and for W1C1 & V1C2 (Figure 34 and 35). Q_{ext} is a function of the frequency ν, the resonator capacity C_κ and length l (5). The coupling ratio of G5A2 crosses the critical coupling $g = 1$ at the 2^{nd} resonance. The chips W1C1 and V1C2 are undercoupled with $g < 0.25 < 1$.

$$g = \frac{Q(n)}{Q_{ext}(\nu, C_\kappa, l) - Q(n)} \tag{20}$$

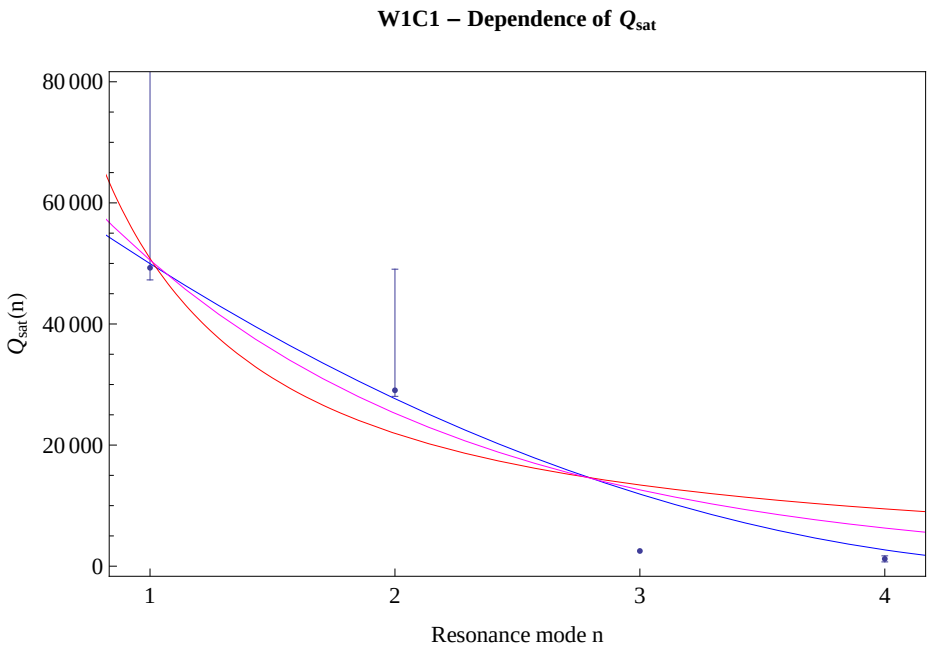

Figure 30: $Q_{sat}(n)$ of W1C1 with quadratic decay (red), exponential decay (violet) and quadratic function (blue). Fit: $a = 101200$, $b = 0.6943$, $c = 50820$, $d = 1.213$, $e = 3274$ and $f = 4.907$.

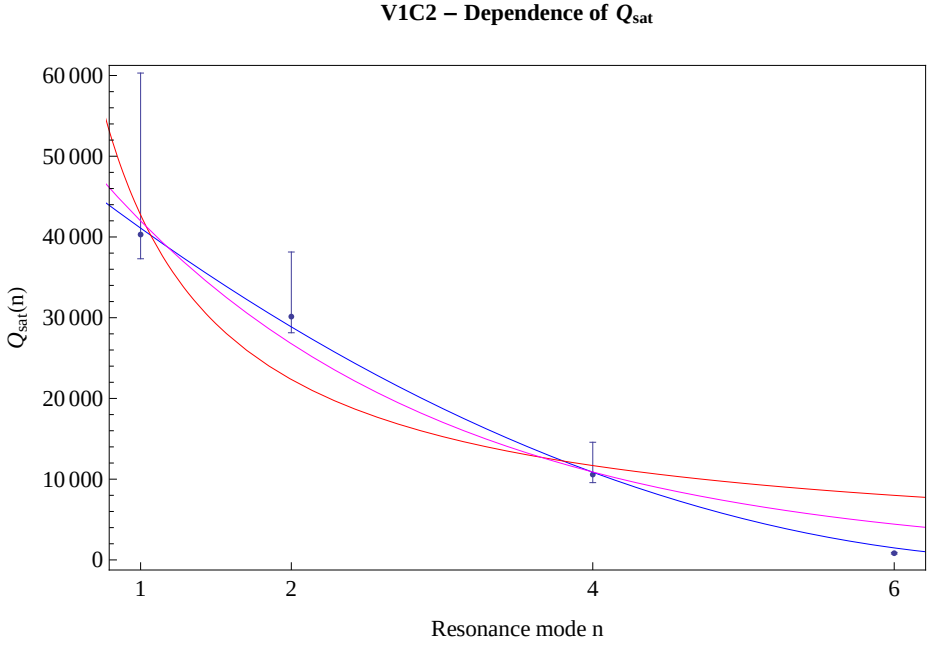

Figure 31: $Q_{sat}(n)$ of V1C2 with quadratic decay (red), exponential decay (violet) and quadratic function (blue). Fit: $a = 65830$, $b = 0.4498$, $c = 42730$, $d = .9353$, $e = 1078$ and $f = 7.174$.

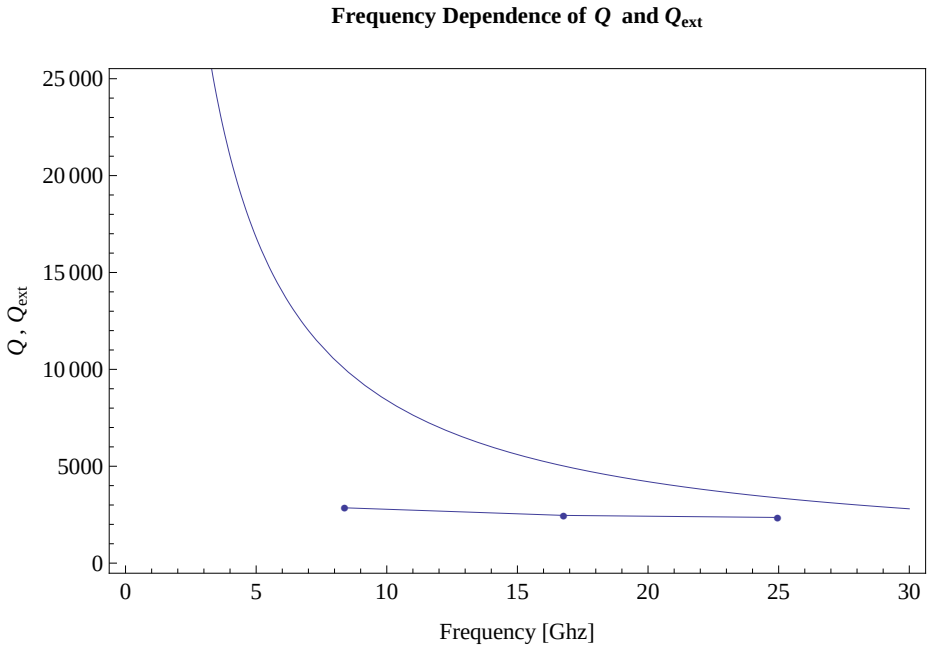

Figure 32: Frequency dependence of the external Q-factor (curve) and Q (points) of G5A2.

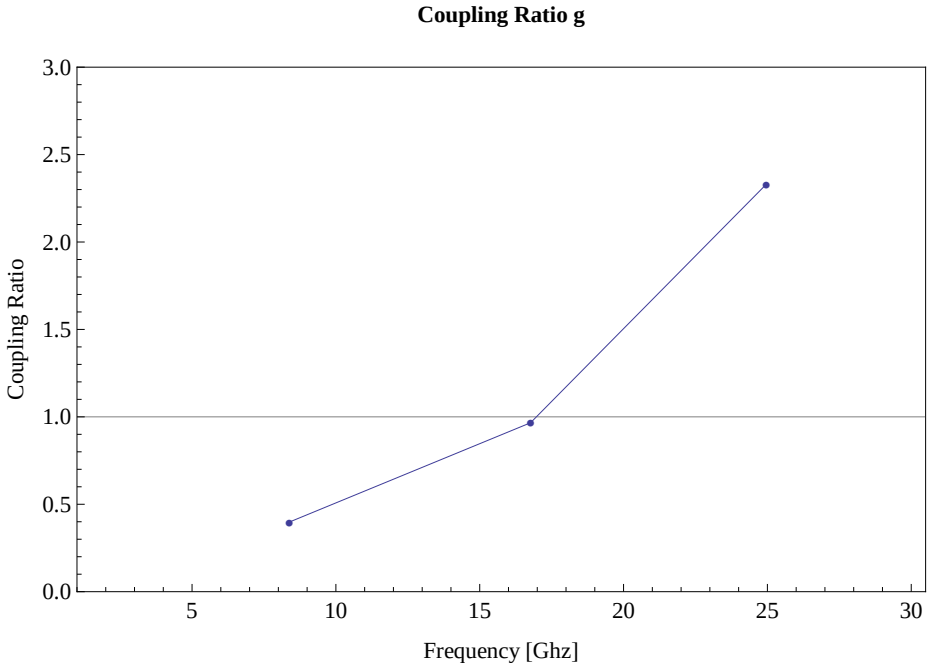

Figure 33: Dependence of the coupling ratio g of G5A2.

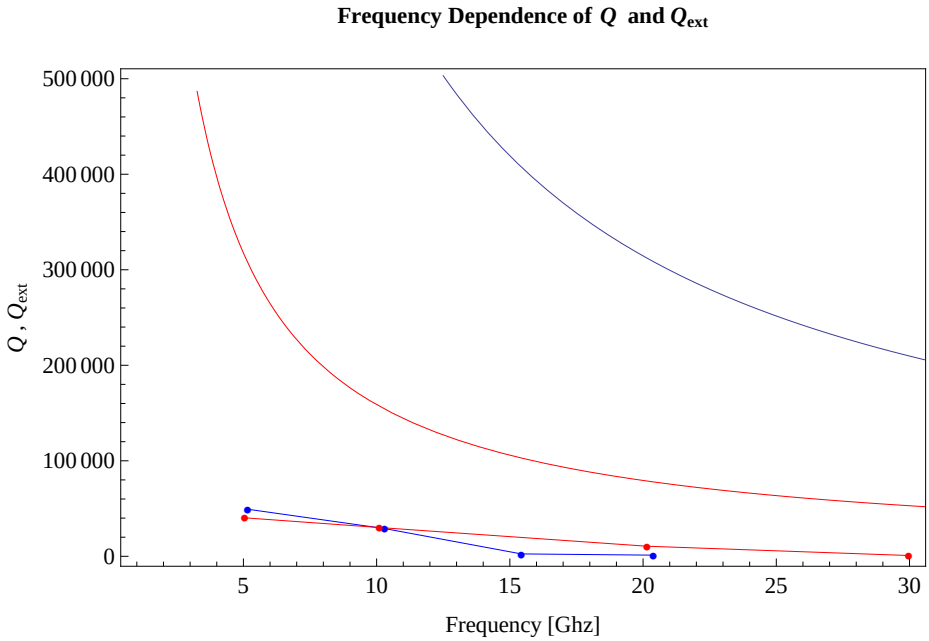

Figure 34: Frequency dependence of the external Q-factor (curve) and Q (points) of W1C1 (blue) and V1C2 (red).

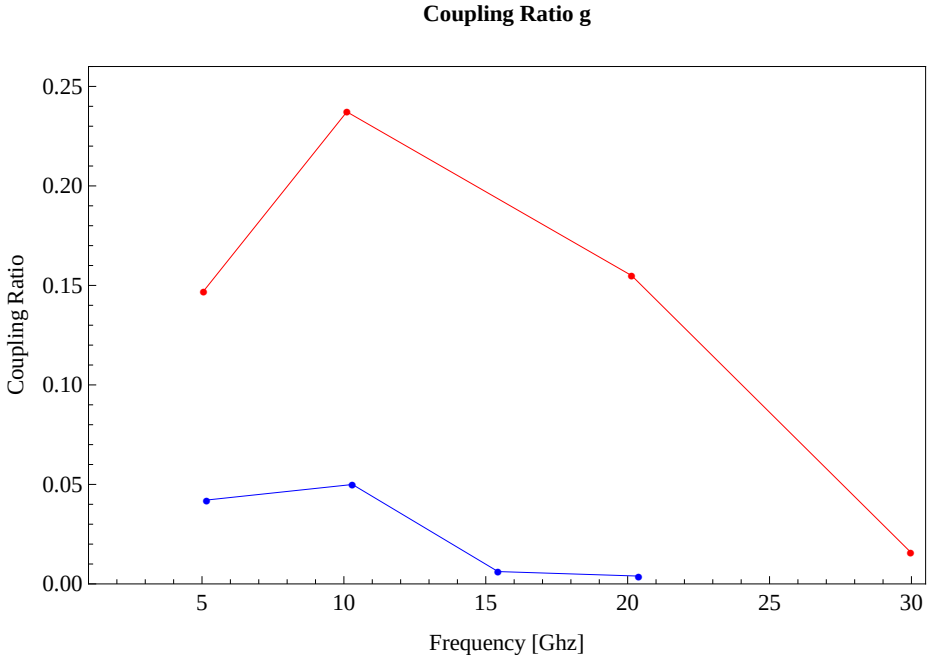

Figure 35: Dependence of the coupling ratio g of W1C1 (blue) and V1C2 (red).

3.6 Temperature Dependence of Resonance Frequency

The temperature dependence of the $\nu 0(T)/\nu 0(T_0)$ is fitted with the function (21). Thereby all resonance mode can be fitted together, each with the same weight.

$$\frac{\nu 0(T)}{\nu 0(T_0)} = \sqrt{\frac{L_l(T_0)}{L_l(T)}} \tag{21}$$

The fitting-parameter are the resistance at the critical temperature $\rho(T_c)$ and the critical temperature T_c. The G5A2 (Figure 37) is fitted separately because it does not match with the W1C1 and V1C2 witch are a newer generation of chips (Figure 38). An upward shift for higher resonance modes was observed. To receive a value for the relative dielectric constant ϵ_r the first resonance of each chip is fitted with (3) and showed in the appendix A. The following values for the fit-parameters are found. The relative dielectric constant for all resonances and chips are shown in Figure 36.

Chip	T_c [K]	$\rho(T_c)$ [$\mu\Omega$m]	ϵ_r
G6A2	13.062	1.049	10.33
W1C1	13.116	0.936	9.21
V1C2			9.43

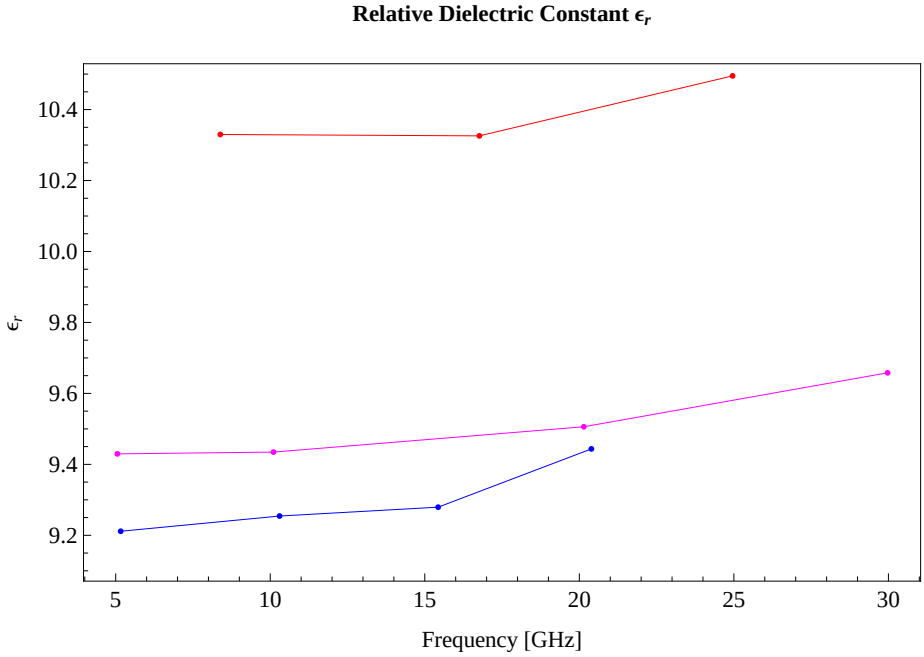

Figure 36: The frequency dependence of the relative dielectric constant ϵ_r of G5A2 (red), W1C1 (blue) and V1C2 (violet).

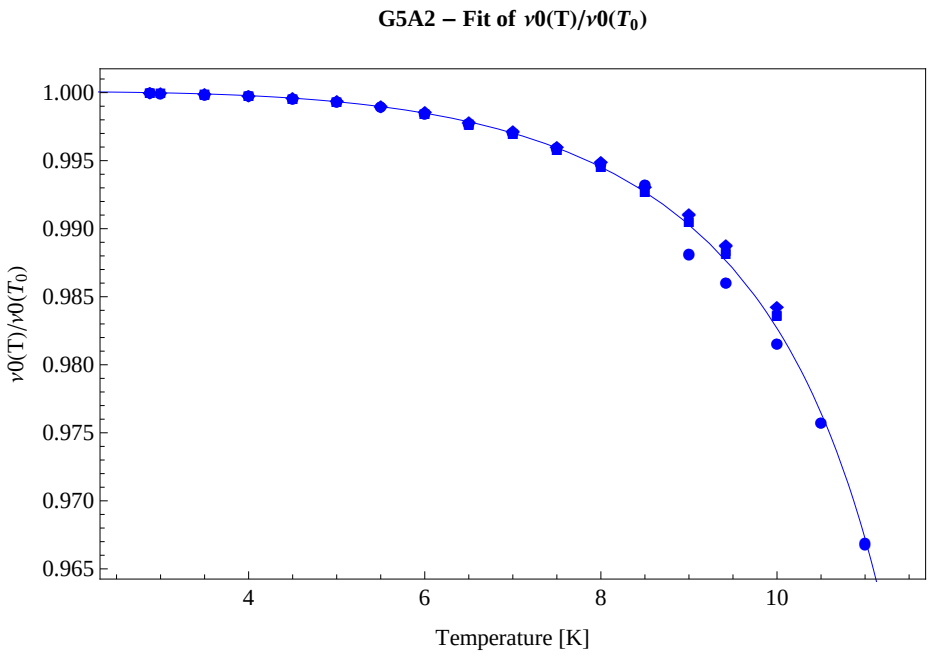

Figure 37: Fit of $\nu 0(T)/\nu 0(T_0)$ of G5A2. • : 1^{st}, ■ : 2^{nd} and ♦ : 3^{rd} resonance. $T_c = 13.0622$ K and $\rho(T_c) = 1.04937 \cdot 10^{-6}$ Ω

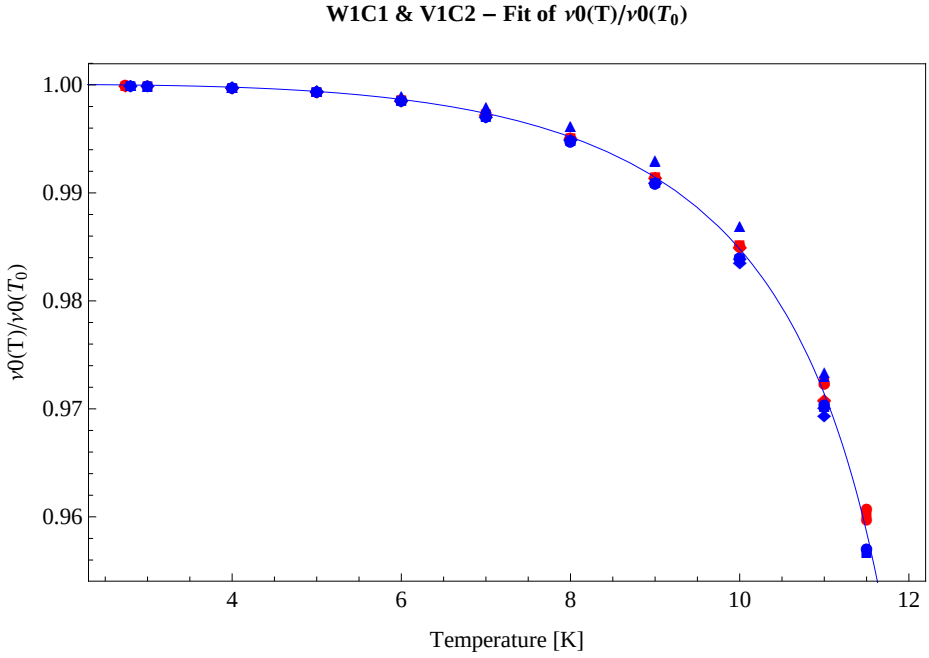

Figure 38: Fit of $\nu 0(T)/\nu 0(T_0)$ of W1C1 (blue: • : 1^{st}, ■ : 2^{nd}, ♦ : 3^{rd} and ▲ : 4^{th} resonance) and V1C2 (red: • : 1^{st}, ■ : 2^{nd} and ♦ : 4^{th} resonance). $T_c = 13.1156$ K and $\rho(T_c) = 9.36451 \cdot 10^{-7}$ Ω.

4 Summary

- With the fit of the transmission a sharp step in the fit-parameter at the critical temperature is visible. The DC-resistance measurement gives a preciser value of the critical temperature.
- Odd resonances, except the first, seem to be double-resonances or are not visible. This could be a result of the asymmetric resonator geometry.
- The Q-factor of the undercoupled resonators saturates for low temperature and decays rather exponential than quadratic. A unphysical quadratic function gives a good fit.
- The fit of $\nu 0(T)$ results in reasonable values for T_c, $\rho(T_c)$ and ϵ_r.

5 Outlook

In the further process of the experiment, the top sample-holder is better isolated with additional sapphire disks to reduce the influence of the temperature oscillations. Thereby the minimum temperature rises. To achieve a lower minimum temperature a shield is added which protects the sample-holder from thermal radiation.

A Plots

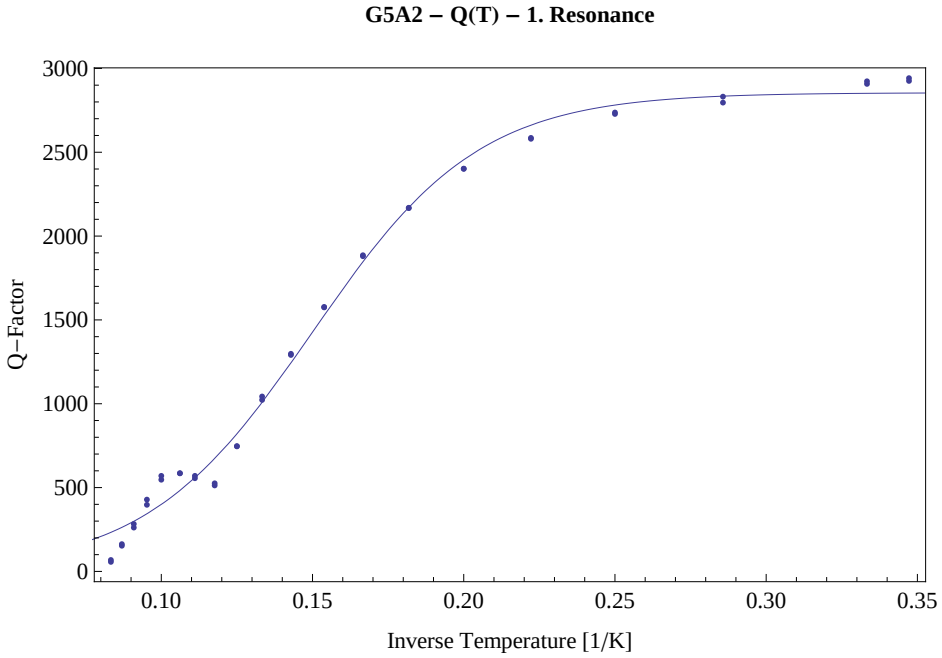

Figure 39: G5A2 - Temperature dependence of the Q-factor. 1. Resonance. Sweep-wise. Fit: $Q_{sat} = 2855.04$, $A = 0.15001$ K^{-1} and $B = 0.0275384$ K^{-1}.

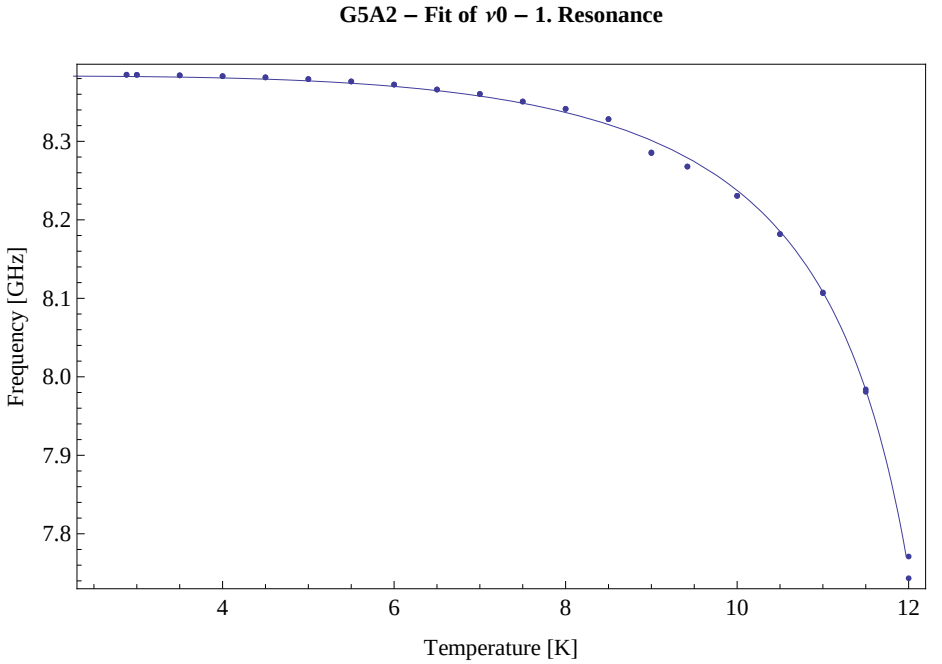

Figure 40: G5A2 - Temperature dependence of $\nu 0$. 1. Resonance. Sweep-wise. $T_c = 13.0622$ K and $\rho(T_c) = 1.04937 \cdot 10^{-6}$ Ω fix. Fit: $\epsilon_r = 10.3298$.

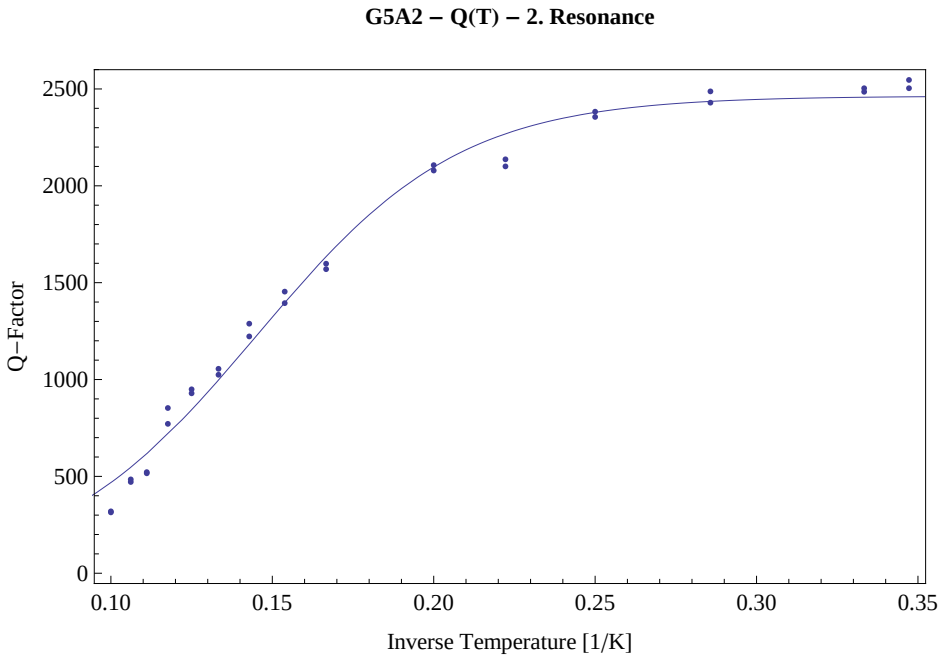

Figure 41: G5A2 - Temperature dependence of the Q-factor. 2. Resonance. Sweep-wise. Fit: $Q_{sat} = 2463.34$, $A = 0.145408$ K^{-1} and $B = 0.031305$ K^{-1}.

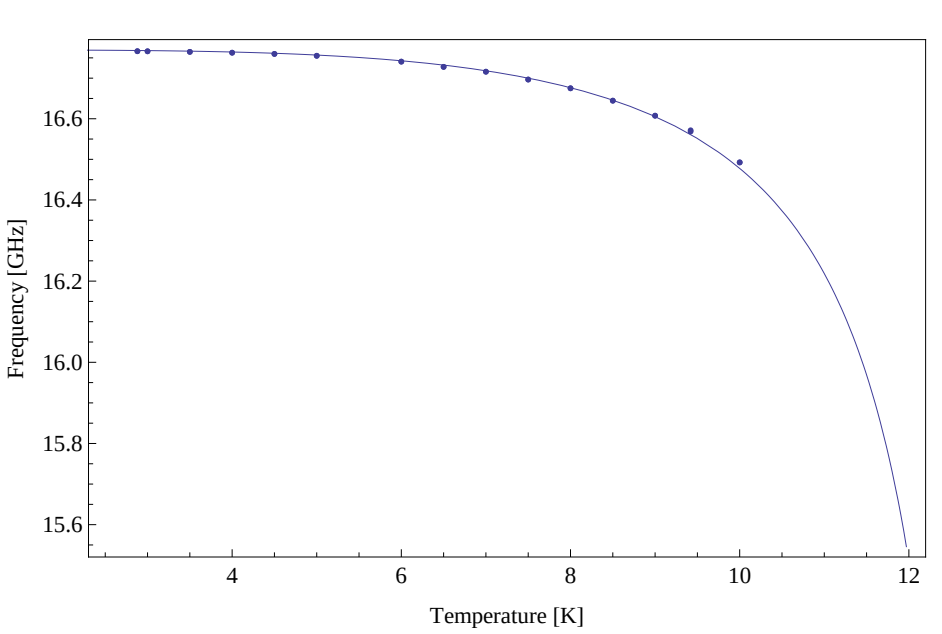

Figure 42: G5A2 - Temperature dependence of $\nu 0$. 2. Resonance. Sweep-wise. $T_c = 13.0622$ K and $\rho(T_c) = 1.04937 \cdot 10^{-6}$ Ω fix. Fit: $\epsilon_r = 10.3259$.

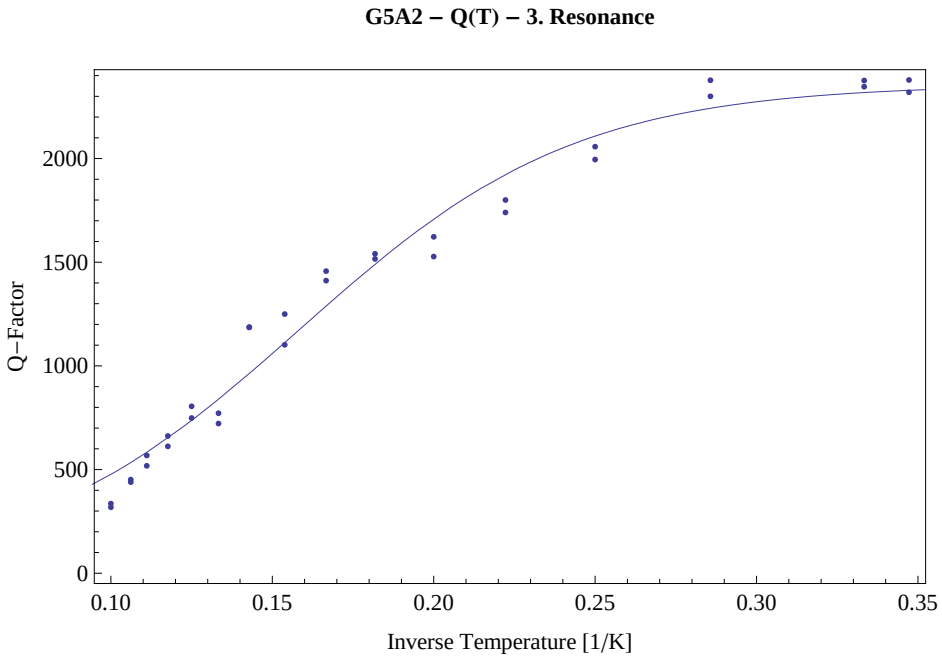

Figure 43: G5A2 - Temperature dependence of the Q-factor. 3. Resonance. Sweep-wise. Fit: $Q_{sat} = 2357.17$, $A = 0.158666$ K^{-1} and $B = 0.0427454$ K^{-1}.

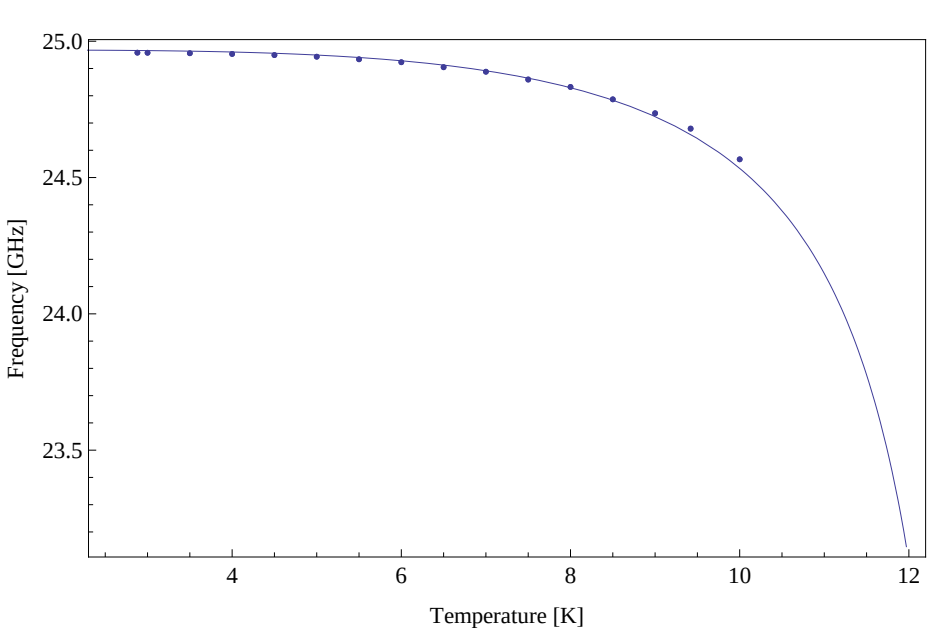

Figure 44: G5A2 - Temperature dependence of $\nu 0$. 3. Resonance. Sweep-wise. $T_c = 13.0622$ K and $\rho(T_c) = 1.04937 \cdot 10^{-6}$ Ω fix. Fit: $\epsilon_r = 10.495$.

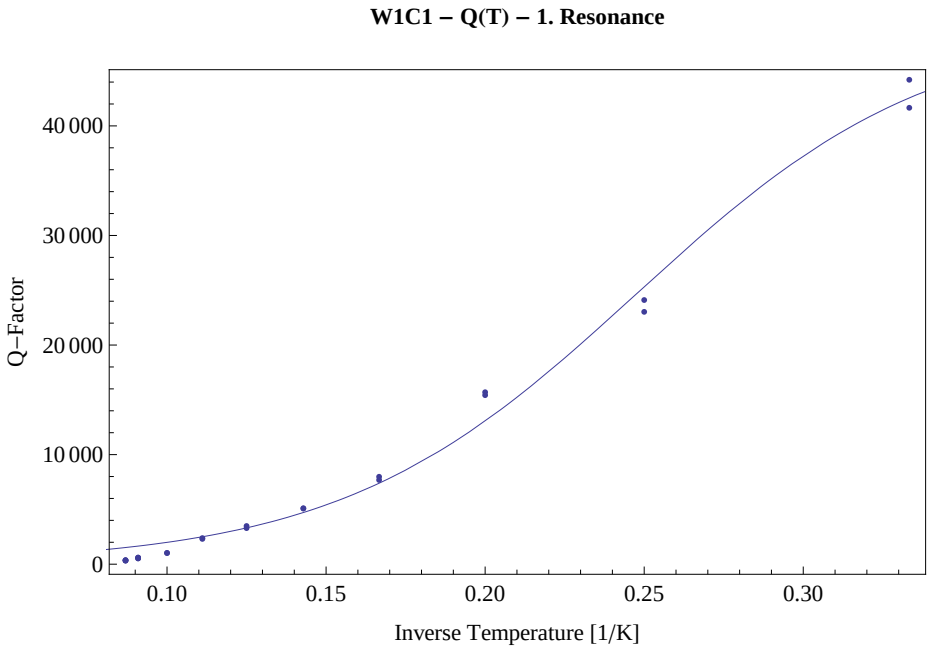

Figure 45: W1C1 - Temperature dependence of the Q-factor. 1. Resonance. Sweep-wise. Fit: $Q_{sat} = 49279.8$, $A = 0.247434$ K^{-1} and $B = 0.0465549$ K^{-1}.

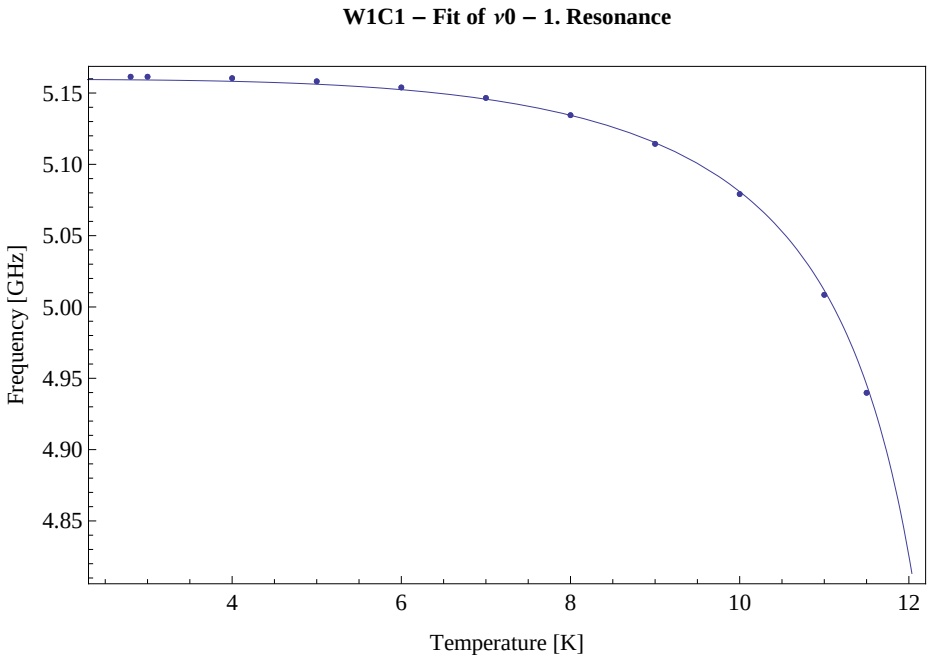

Figure 46: W1C1 - Temperature dependence of $\nu 0$. 1. Resonance. Sweep-wise. $T_c = 13.1156$ K and $\rho(T_c) = 9.36451 \cdot 10^{-7}$ Ω fix. Fit: $\epsilon_r = 9.2114$.

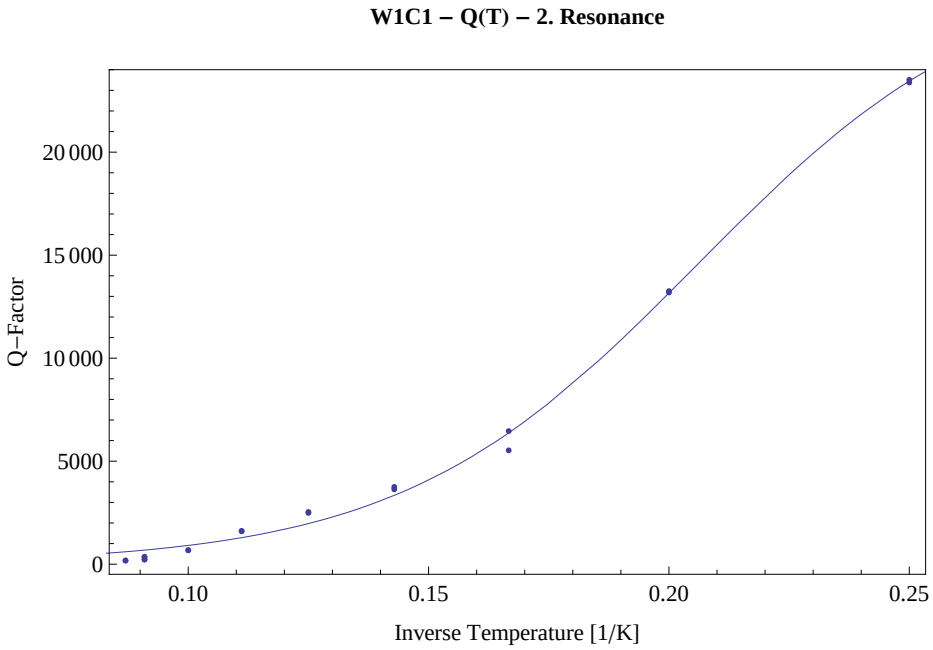

Figure 47: W1C1 - Temperature dependence of the Q-factor. 2. Resonance. Sweep-wise. Fit: $Q_{sat} = 29050.6$, $A = 0.205825$ K^{-1} and $B = 0.0308466$ K^{-1}.

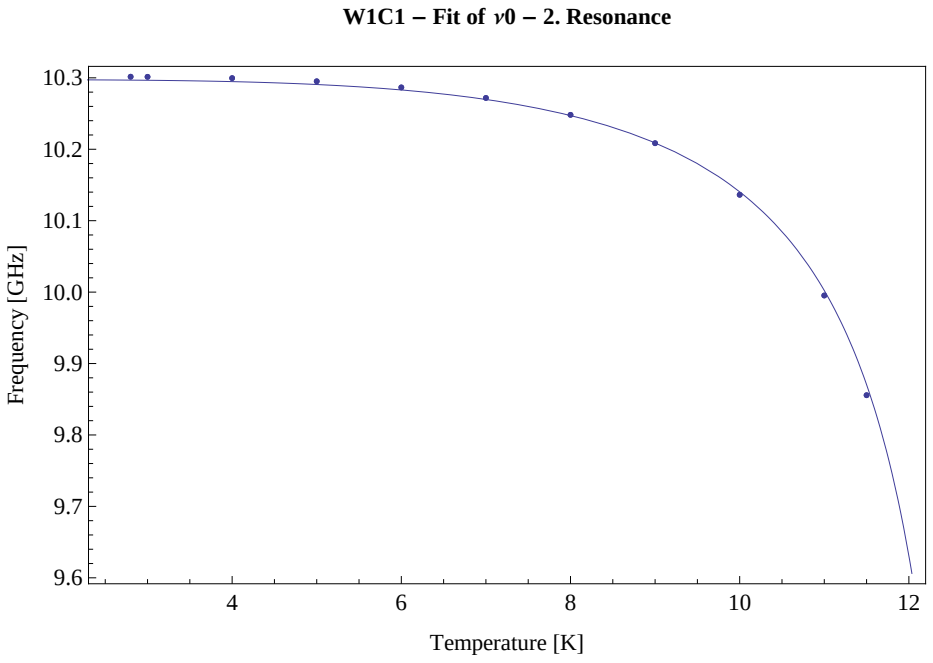

Figure 48: W1C1 - Temperature dependence of $\nu 0$. 2. Resonance. Sweep-wise. $T_c = 13.1156$ K and $\rho(T_c) = 9.36451 \cdot 10^{-7}$ Ω fix. Fit: $\epsilon_r = 9.25434$.

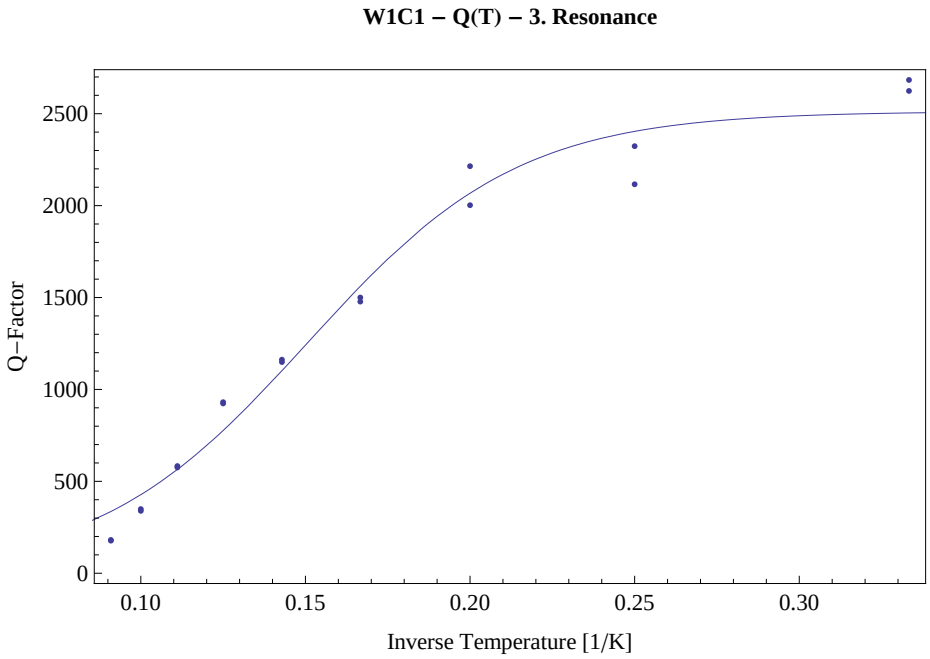

Figure 49: W1C1 - Temperature dependence of the Q-factor. 3. Resonance. Sweep-wise. Fit: $Q_{sat} = 2512.62$, $A = 0.150792$ K^{-1} and $B = 0.0320404$ K^{-1}.

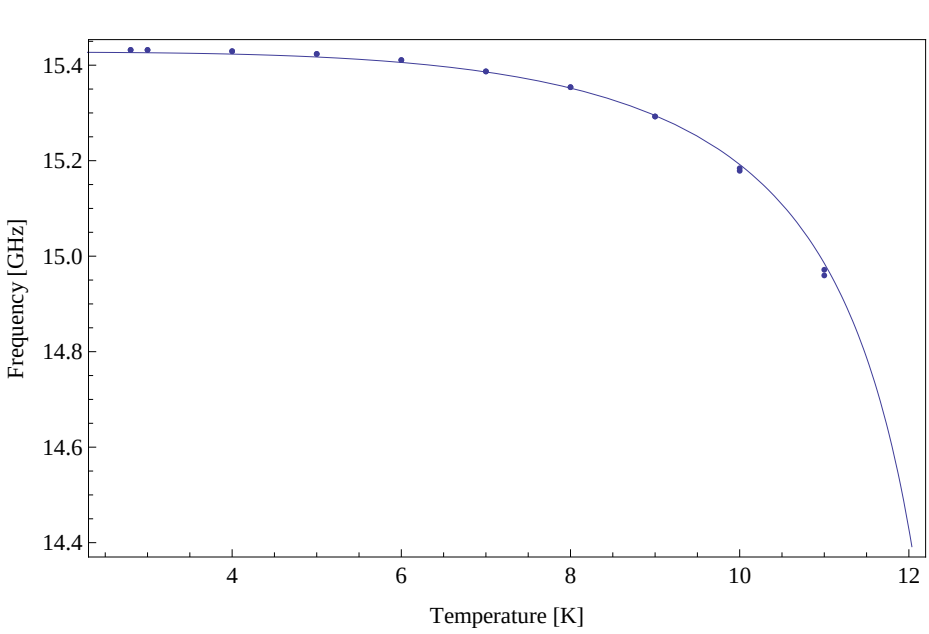

Figure 50: W1C1 - Temperature dependence of $\nu 0$. 3. Resonance. Sweep-wise. $T_c = 13.1156$ K and $\rho(T_c) = 9.36451 \cdot 10^{-7}$ Ω fix. Fit: $\epsilon_r = 9.27931$.

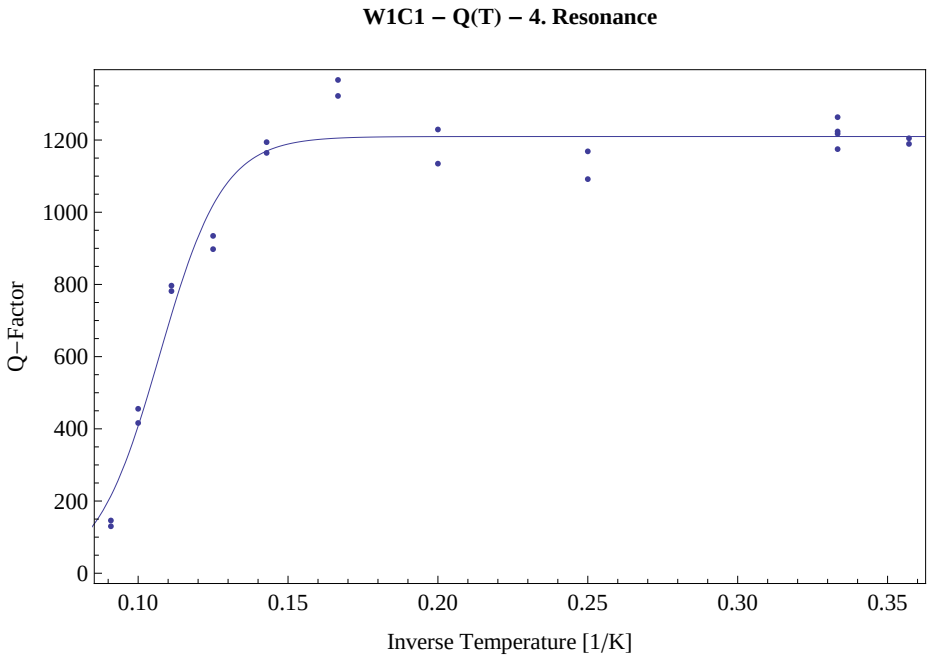

Figure 51: W1C1 - Temperature dependence of the Q-factor. 4. Resonance. Sweep-wise. Fit: $Q_{sat} = 1209.72$, $A = 0.107178$ K^{-1} and $B = 0.107178$ K^{-1}.

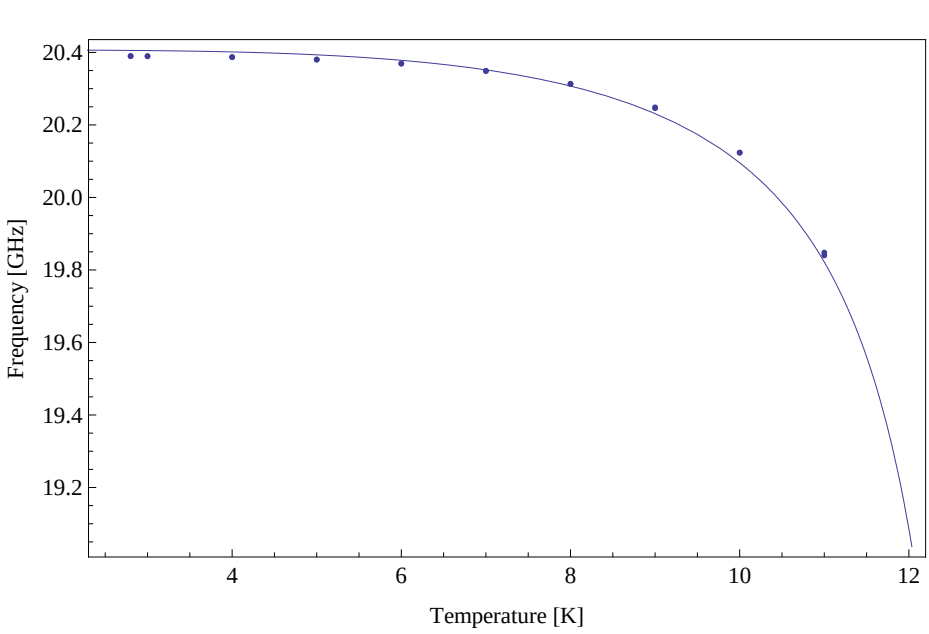

Figure 52: W1C1 - Temperature dependence of $\nu 0$. 4. Resonance. Sweep-wise. $T_c = 13.1156$ K and $\rho(T_c) = 9.36451 \cdot 10^{-7}$ Ω fix. Fit: $\epsilon_r = 9.44357$.

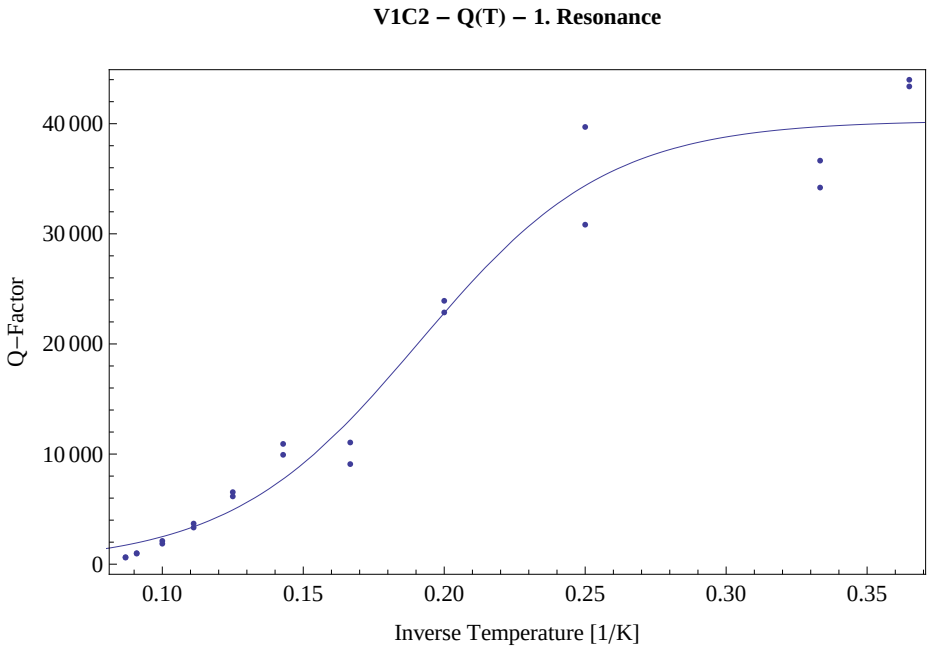

Figure 53: V1C1 - Temperature dependence of the Q-factor. Resonance. Point-wise. Fit: $Q_{sat} = 40301.3$, $A = 0.191062$ K^{-1} and $B = 0.0335186$ K^{-1}.

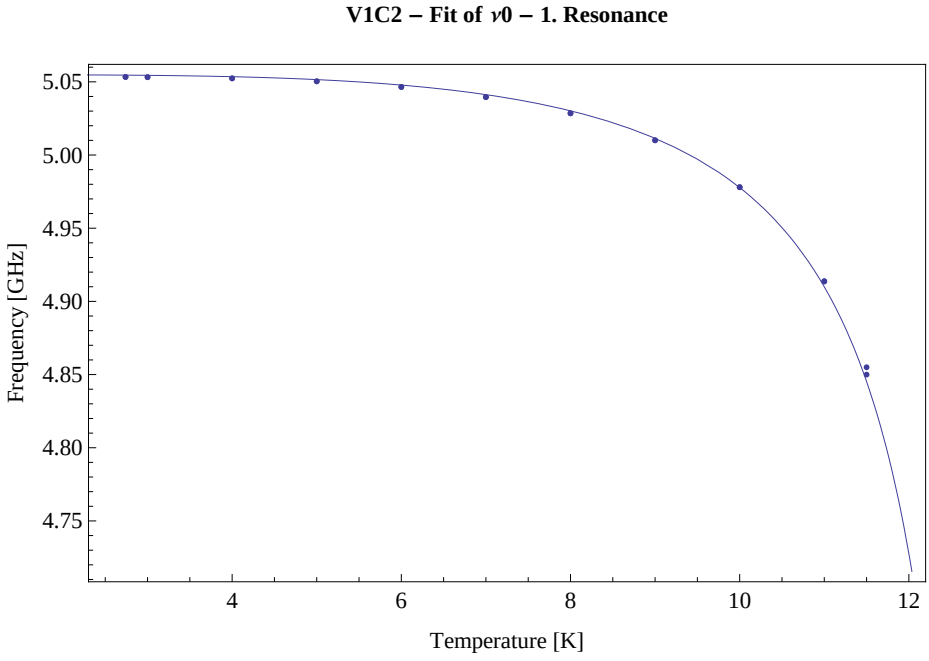

Figure 54: V1C1 - Temperature dependence of $\nu 0$. 1. Resonance. Point-wise. $T_c = 13.1156$ K and $\rho(T_c) = 9.36451 \cdot 10^{-7}$ Ω fix. Fit: $\epsilon_r = 9.42955$.

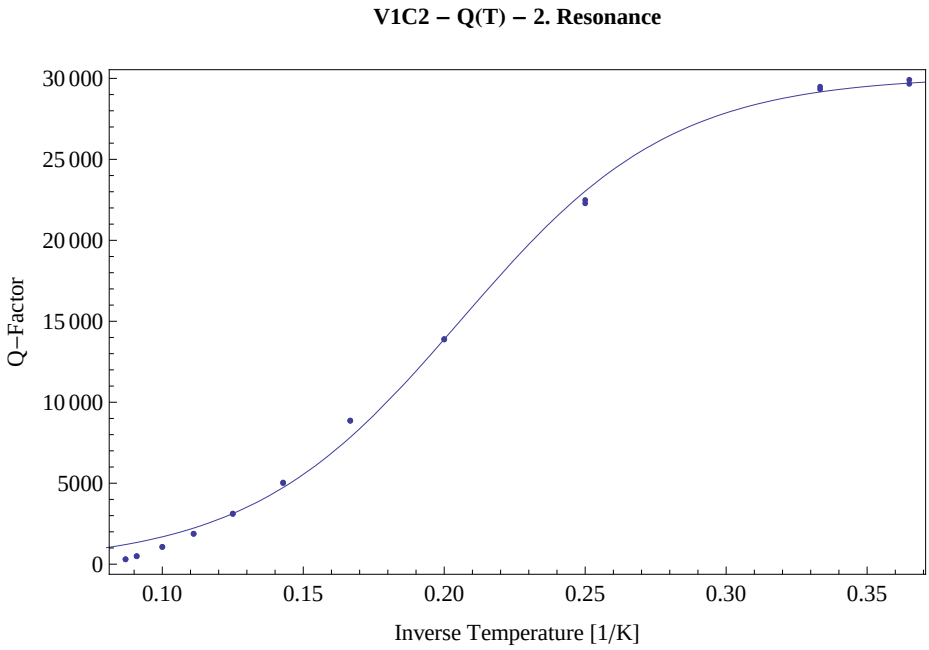

Figure 55: V1C1 - Temperature dependence of the Q-factor. Resonance. Point-wise. Fit: $Q_{sat} = 30136.5$, $A = 0.205885$ K^{-1} and $B = 0.0374986$ K^{-1}.

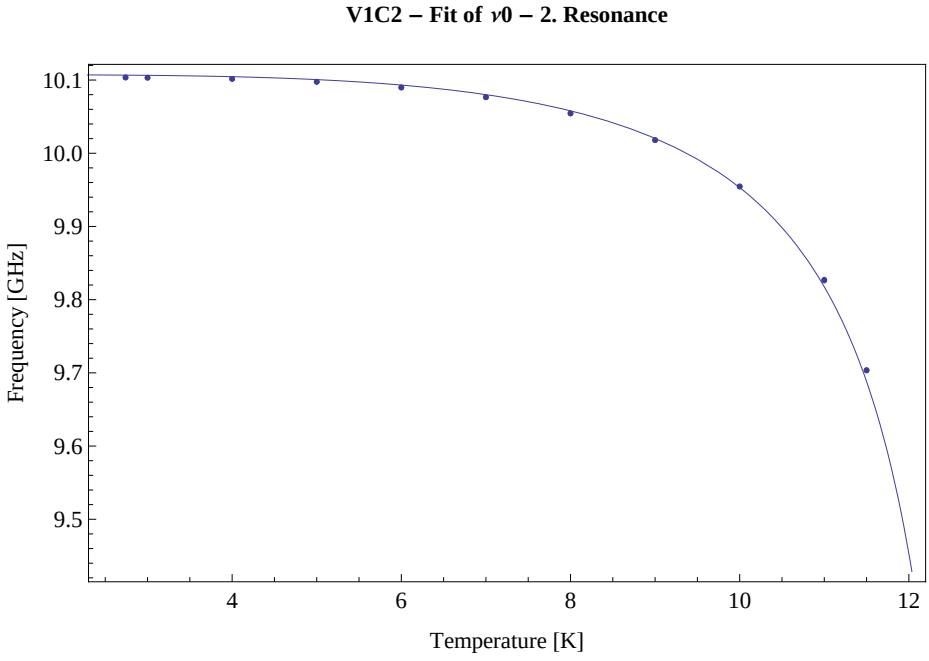

Figure 56: V1C1 - Temperature dependence of $\nu 0$. 2. Resonance. Point-wise. $T_c = 13.1156$ K and $\rho(T_c) = 9.36451 \cdot 10^{-7}$ Ω fix. Fit: $\epsilon_r = 9.43454$.

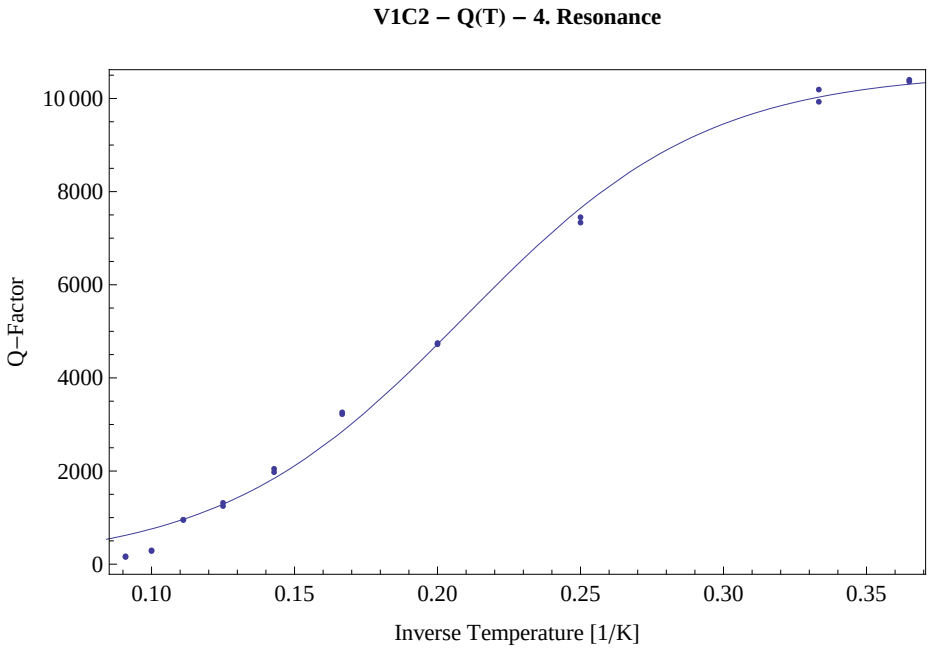

Figure 57: V1C1 - Temperature dependence of the Q-factor. 4. Resonance. Point-wise. Fit: $Q_{sat} = 10572.4$, $A = 0.209129$ K^{-1} and $B = 0.0425901$ K^{-1}.

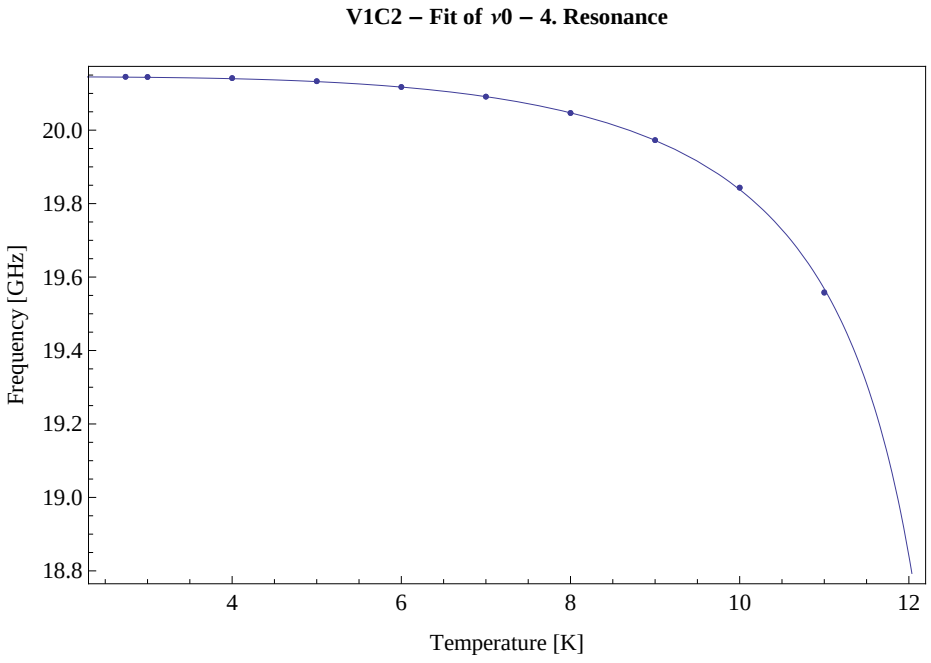

Figure 58: V1C1 - Temperature dependence of $\nu 0$. 4. Resonance. Point-wise. $T_c = 13.1156$ K and $\rho(T_c) = 9.36451 \cdot 10^{-7}$ Ω fix. Fit: $\epsilon_r = 9.50597$.

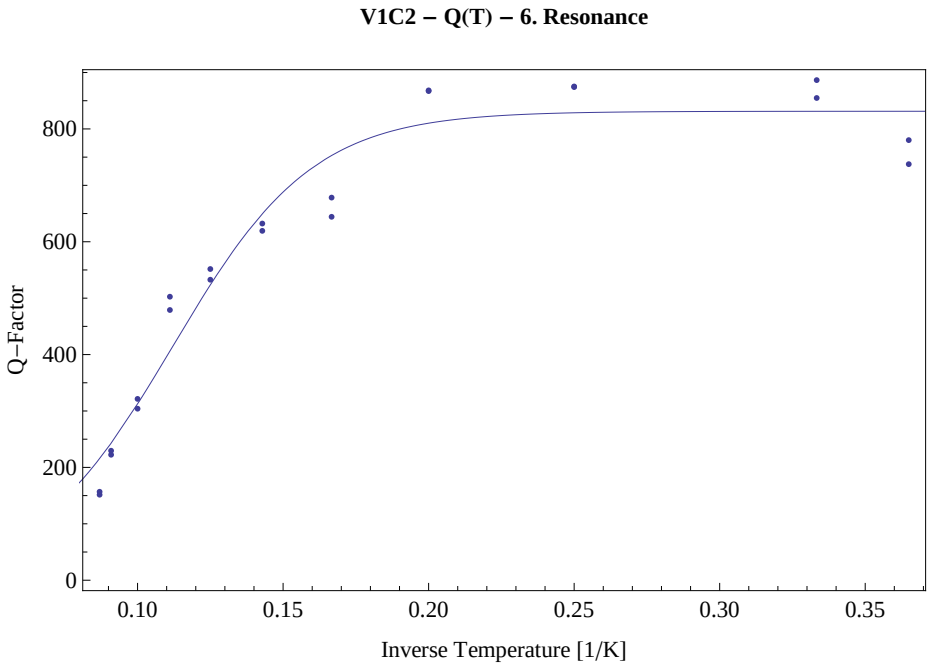

Figure 59: V1C1 - Temperature dependence of the Q-factor. 6. Resonance. Point-wise. Fit: $Q_{sat} = 831.318$, $A = 0.112215$ K^{-1} and $B = 0.0240747$ K^{-1}.

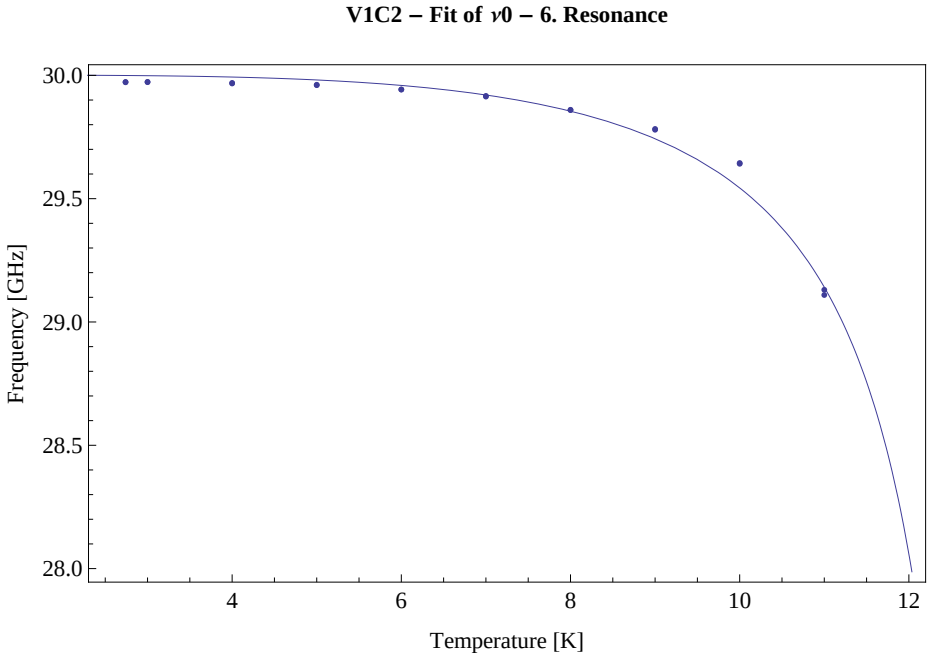

Figure 60: V1C1 - Temperature dependence of $\nu 0$. 6. Resonance. Point-wise. $T_c = 13.1156$ K and $\rho(T_c) = 9.36451 \cdot 10^{-7}$ Ω fix. Fit: $\epsilon_r = 9.65802$.

B Mathematica Codes

Function to convert the time-stamp of LabView to Mathematica:

```
ConvertDate[data_] :=
 MapThread[Join[{#1}, #2] &, {MapThread[
    DateList[StringJoin[#1, " ", #2]] &, {data[[All, 1]],
     data[[All, 2]]}], data[[All, Range[3, Length[data[[1]]]]]]}]
ConvertData=ConvertDate[{{"2012/02/17", "18:57:33.19",...},...}]
{{{2012,2,17,18,57,33.19`},...},...}
DateListPlot[ConvertData]
```

Function to saparate the left and the right curve:

```
separation[data_] :=
 Module[{step, length, i, k1, k2, min, max, j, dataleft, dataright
    },
  step = 16;
  length = Length[data];
  For[i = 1; k1 = 1; k2 = 1; min = {{0, 0}, {0, 0}};
   max = {{0, -1000}, {0, -1000}};
   datamax = Table[Table[-1000, {i, 1, 2}], {j, 1, length}];
   datamin = Table[Table[0, {i, 1, 2}], {j, 1, length}];,
   i <= length,
   i++,
   min[[Mod[i, 2]]] = {0, 0}; max[[Mod[i, 2]]] = {0, -1000};
   For[j = -Ceiling[step/2], j <= Floor[step/2], j++,
    If[1 <= i + j <= length,
     If[data[[i + j, 2]] >= max[[Mod[i, 2], 2]],
      max[[Mod[i, 2]]] = data[[i + j]]];
     If[data[[i + j, 2]] <= min[[Mod[i, 2], 2]],
      min[[Mod[i, 2]]] = data[[i + j]]];
     ]
    ];
   If[i == 1,
    datamax[[1]] = max[[1]]; datamin[[1]] = min[[1]],
    If[max[[Mod[i + 1, 2], 2]] != max[[Mod[i, 2], 2]], k1++;
     datamax[[k1]] = max[[Mod[i, 2]]]];
    If[min[[Mod[i + 1, 2], 2]] != min[[Mod[i, 2], 2]], k2++;
     datamin[[k2]] = min[[Mod[i, 2]]]]
    ]
   ];
  datamax = Take[datamax, k1];
  datamin = Take[datamin, k2];
  pmin = Position[datamin[[All, 2]], Max[datamin[[All, 2]]]
    [[1, 1]]];
  dataleft =
   Join[Select[datamax[[All]], #[[1]] < datamin[[pmin, 1]] &],
    datamin[[pmin ;;]]];
  dataright =
   Join[datamin[[1 ;; pmin]],
    Select[datamax[[All]], #[[1]] > datamin[[pmin, 1]] &]]
  ]
```

Function to fit the resonance from Raphael [8]:

```
FitLorentz[data_] := Module[{dbList, dataMax, threedb, threedbList
   , Qstart, fitData, fitparams},
  (* define lorentzian function which is to be fitted to data *)
  Lfunc = att/(2 Pi Q v0) 1/((x/v0 - 1)^2 + 1/4 (1/Q)^2);
  (* create data list in normal scale *)
  fitData =
   Table[{data[[i, 1]], 10^(data[[i, 2]]/10)}, {i, Length[data]}];
  (* find start parameters *)
  (* create S list *)
  dbList  = Table[fitData[[i]][[2]], {i, fitData // Length}];
  (* astart & vstart from maximum *)
  dataMax = fitData[[First[First[Position[fitData, Max[dbList
      ]]]]]];
  (* find Q, start by getting all values above three db *)
  threedb = dataMax[[2]]/2;
  threedbList = Cases[dbList, x_?(#1 > threedb &)];
  (* first and last element will result in delta omega *)
  Qstart = dataMax[[1]]/(data[[First[First[Position[dbList,
    threedbList // Last]]]]][[1]] - data[[First[First[
    Position[dbList, threedbList // First]]]]][[1]]);
  (* set starting parameters *)
  fitparams = {{att, (Pi*dataMax[[1]]*dataMax[[2]])/(
     2*Qstart)}, {v0, dataMax[[1]]}, {Q, Qstart}};
  FindFit[fitData, Lfunc, fitparams, x, PrecisionGoal -> 15,
   AccuracyGoal -> 3]
  ]
```

Modified function to fit in dB:

```
FitLorentzdB[data_] := Module[{dbList, dataMax, threedb,
    threedbList,
   Qstart, fitData, fitparams},
  LfuncdB =
   10*Log[10, att/(2 Pi Q v0) 1/((x/v0 - 1)^2 + 1/4 (1/Q)^2)];
  fitData =
   Table[{data[[i, 1]], 10^(data[[i, 2]]/10)}, {i, Length[data]}];
  dbList  = Table[fitData[[i]][[2]], {i, fitData // Length}];
  dataMax = fitData[[First[First[Position[fitData, Max[dbList
      ]]]]]];
  threedb = dataMax[[2]]/2;
  threedbList = Cases[dbList, x_?(#1 > threedb &)];
  Qstart = dataMax[[1]]/(data[[First[First[Position[dbList,
    threedbList // Last]]]]][[1]] - data[[First[First[
    Position[dbList, threedbList // First]]]]][[1]]);
  fitparams = {{att, (Pi*dataMax[[1]]*dataMax[[2]])/(
     2*Qstart)}, {v0, dataMax[[1]]}, {Q, Qstart}};
  FindFit[data, LfuncdB, fitparams, x, PrecisionGoal -> 15,
   AccuracyGoal -> 3]
  ]
```

References

[1] A. Wallraff, *"Hybrid Cavity Quantum Electrodynamics with Atoms and Circuits"*, 2008.

[2] M. Goeppl, A. Fragner, M. Baur, R. Bianchetti, S. Filipp, J. M. Fink, P. J. Leek, G. Puebla, L. Steffen, and A. Wallraff, Journal of applied Physics **104**, 113904 (2008).

[3] K. Watanabe, K. Yoshida, T. Aoki, and S. Kohjiro, *Kinetic Inductance of Superconducting Coplanar Waveguides*, Japanese Journal of Applied Physics, Vol. 33, Issue 10, pp. 5708 (1994).

[4] T. Gallagher, *"Rydberg atoms"*, Cambridge University Press, 1994.

[5] S. D. Hogan, J. A. Agner, F. Merkt, T. Thiele, S. Filipp, and A. Wallraff, Physical Review Letters **108**, 063004 (2012).

[6] LakeShore, *"User's Manual Model 340 Temperature Controller"*, 2009.

[7] E.D. Marquardt, J.P. Le, and R. Radebaugh, in *11^{th} International Cryocooler Conference*, Keystone, Co , 2000.

[8] R. Barmettler, Master thesis, ETH Zurich, 2012.

[9] Rainee N. Simons, Coplanar Waveguide Circuits Components and Systems, Wiley-IEEE Press, 2001.

[10] Microwave Encyclopedia, *"Coax loss calculations"* [Online], 4 June 2012, http://www.microwaves101.com/encyclopedia/coaxloss.cfm.

[11] L. Frunzio, A. Wallraff, D. Schuster, J. Majer, and R. Schoelkopf, *"Fabrication and Characterization of Superconducting Circuit QED Devices for Quantum Computation"*, IEEE Transactions on applied Superconductivity, Vol. 15, No. 2, pp. 860863, June 2005.